Enhancer priming enables fast and sustained transcriptional responses to Notch signaling

Julia Falo-Sanjuan[1], Nick Lammers[2], Hernan Garcia[2], Sarah Bray[1],

1 Department of Physiology, Development and Neuroscience. University of Cambridge

2 Department of Physics. University of California, Berkeley

*** correseponding@author.mail**

Abstract

Information from developmental signaling pathways must be accurately decoded to generate the appropriate transcriptional outcomes. Despite the highly conserved Notch receptor having the unusual feature that its intracellular domain (NICD) transduces the signal directly to the nucleus, we know little about how enhancers decipher NICD in the real time of developmental decisions. Using the MS2/MCP system to visualize nascent transcripts in *Drosophila* embryos we reveal how Notch activity is read by two target enhancers to produce highly synchronized and sustained profiles of transcription in a stripe of mesectoderm (MSE) cells. Two key principles are uncovered by manipulating the levels of NICD and by altering specific motifs within the enhancers. First, NICD levels alter transcription by increasing the bursting size rather than frequency. Second, priming of MSE enhancers by localized transcription factors is required for NICD to confer synchronized and sustained activity; in their absence, MSE enhancers confer stochastic bursty transcription profiles. The dynamic response of an individual enhancer to NICD can thus differ depending on which other transcription factors are present. We propose that priming mechanisms render enhancers differentially sensitive to signals and will be of major importance when a rapid and robust transcriptional response is needed.

Introduction

Genes respond to external and internal cues through the action in the nucleus of transcription factors and effectors of signalling pathways. Regulatory regions that surround genes, termed enhancers, integrate the information from

these inputs to produce an appropriate transcriptional output. During development some of these decisions can occur in a matter of minutes, but usually the outcomes are measured many hours later. Rarely has transcription dynamics been analyzed *in vivo* in the real-time of the developmental signalling pathways, so we know little about how recipient enhancers decipher the signals. For example, how are signalling properties such as duration, fold-change detected and what impact do these have on the transcription profiles produced?

With the advent of precise and quantitative methods to measure transcription, such as single molecule in situ hybridization (smFISH) or live imaging, it has become evident that transcription is not a continuous process. Instead, genes that are being actively transcribed undergo bursts of initiation that are separated by inactive intervals [15, 25]. Indeed in a time-lapse analysis of 8000 individual human genomic loci, episodic bursting, rather than continuous expression, predominated at virtually all loci [17]. This bursting phenomenon means that the overall transcriptional output can be modulated by changing either the frequency with which a burst occurs (measured by the gap between bursts) or the size of each burst (measured by changes in burst duration and/or the rate of initiation). In the human study, burst frequency was modulated at loci with weaker expression and burst size at more strongly expressed genes [17]. In most other cases analyzed, the major mode of regulation by enhancers has been through changes in bursting frequency rather than burst size. For example, enhancers for early patterning genes in *Drosophila* embryos all produce similar bursting size but have different bursting frequencies, which can be attenuated by the presence of insulators [21]. Similarly, steroids increase the bursting frequency of target enhancers to regulate their activation kinetics [20, 32]. Since an increase in burst frequency occurred when the beta-globin enhancer was forced to loop to the promoter [2], it has been proposed that the dynamics of interactions between the enhancers and promoter could be responsible for driving the bursting frequency. So far however we have little understanding whether this underpins the dynamics of transcription nor what properties are modulated by developmental signals to confer appropriate outputs in an *in vivo*, developing organism.

Transcriptional bursting is thought to make an important contribution to cellular diversity by favouring heterogeneity in the timings and levels of transcriptional activity between cells [44]. For example, in cells exposed to estrogen, response times for activation of transcription measured live were highly variable and there was no coherent cycling between active and inactive states [20]. Such stochastic transcriptional behaviour has been found of key importance in many developmental decisions, such as the differentiation of photoreceptors in the *Drosophila* eye [50], hematopoietic cell differentiation in mouse cells [12, 42] or during neuronal differentiation in the zebrafish retina [8]. But while an attractive feature for promoting heterogeneity, such variability in responses could be extremely disruptive in developmental processes where the coordinated response of many cells is required to pattern specific structures. In some cases this maybe circumvented by mechanisms that allow cells to achieve the same average mRNA output and so produce homogeneous patterns of gene expression [34]. For example, cells that

express the mesodermal determinant Snail average their transcriptional output by mRNA diffusion to produce a homogeneous field of cells and a sharp boundary [10]. However it is only in rare circumstances that mRNA diffusion can operate and it is unclear whether other averaging mechanisms would be effective over shorter time intervals. To effectively achieve reproducible patterns, cells must therefore overcome the variability that is inherent in transcriptional bursting and stochastic enhancer activation.

Notch signaling is one highly conserved developmental signaling pathway that is deployed in multiple different contexts. It has the unusual feature that the Notch intracellular domain (NICD) transduces the signal directly to the nucleus, when it is released by a series of proteolytic cleavages precipitated by interactions with the ligands. NICD then stimulates transcription by forming a complex with the DNA binding protein CSL and the co-activator Mastermind (Mam) [11]. The lack of amplification makes this a powerful system to investigate how signals are deciphered by responding enhancers. Furthermore, there may be differences in the levels and dynamics of NICD produced by different ligands [41]. However, although its role as a transcriptional activator is well established, at present we know little about how enhancers respond to NICD in the real time of developmental decisions. For example, we do not know whether NICD, like other factors, modulates bursting frequency nor whether it functions as an ON toggle switch or a rheostat. Nor do we know what features of the responding enhancer confer the output properties, although current dogma argues that paired CSL sites (referred to as SPS motifs) [1, 40] whose precise spacing could favour NICD-NICD dimerization, yield the strongest responses [40].

In order to determine how enhancers respond to Notch activity in real time we have used the MS2/MCP system to visualize nascent transcripts in *Drosophila* embryos. To do so we used two well-characterised Notch responsive enhancers that drive expression in a stripe of mesectoderm (MSE) cells and analyzed the levels of transcription they produced over time at the single cell level. Strikingly their activity was highly synchronized, with all MSE cells initiating transcription within a few minutes of one another, and once active, they produced sustained profiles of transcription. By manipulating the levels of NICD and altering key motifs within the enhancers we uncover two key principles. First, the ability of NICD to confer synchronized and sustained activity in MSE requires that the enhancers are primed by localized transcription factors. In their absence, MSE enhancers confer stochastic bursty transcription profiles, demonstrating that different response profiles can be generated from a single enhancer according to which other factors are present. Second, changing Notch levels modulates the transcription burst size but not length of the periods between bursts, in contrast to most current examples for enhancer activation. These two key concepts that we have uncovered by analysing the dynamics of transcription profiles produced by enhancer variants in different signalling conditions are likely to be of general importance for gene regulation by other signalling pathways in developmental and disease contexts.

Results

Synchronised and sustained enhancer activation in response to Notch

To investigate how Notch signals are read out in real time, we focused on the well-characterized mesectodermal enhancers (MSEs) from the *Enhancer of split-Complex (E(spl)-C)* (known as *m5/m8*) and from *singleminded* (*sim*) [16,39,52]. These direct expression in two stripes of cells when Notch is activated in response to Delta signals from the presumptive mesoderm (Fig. 1**AB**) [38]. To visualize transcription from these enhancers in real time, they were inserted into MS2 reporter constructs containing the promoter from the gene *even-skipped* (*peve*), 24 *MS2* loops and the *lacZ* transcript (Fig. 1**A**). When these *MS2* reporters are combined with MCP-GFP in the same embryos, nascent transcription is marked by the accumulation of MCP-GFP in bright nuclear puncta, where the total fluorescence in each spot is directly proportional to the number of transcribing mRNAs at any timepoint (Fig. 1**AB**) [22]. In this way the levels of transcription can be followed over time at the single cell level by tracking the puncta relative to the nuclei (which were labelled with His2Av-RFP).

The MSE cells, which form CNS midline precursors similar to the vertebrate floorplate, are established during nuclear cycle 14 (nc14) of embryogenesis. At this stage both *m5/m8* and *sim* direct expression in two one-cell wide stripes flanking the mesoderm (Fig.1**C**) [52], that converge to the midline during gastrulation. Visualizing transcription in real time revealed that all cells along the MSE stripe switch on the reporter transcription within a narrow time-window ($\sim$ 5-10 min) (Fig. 1**CDE**). We note that both enhancers also directed transcription in broad domains in nuclear cycles 10 to 13 (**Movie 1. Movie 2.**) and that there was an initial burst of activity in the first few minutes of nuclear cycle 14. However, this was followed by a long period (approximately 20 min) of inactivity before the cells in the MSE stripe initiated transcription concurrently.

Both enhancers were then active in a continuous manner - few separated bursts of transcription were detected - throughout the remaining period of nc14 as the embryos underwent the first stage of gastrulation (mesoderm invagination) (Fig. S1**E**). Although continuous, there were nevertheless fluctuations in the levels of activity from each transcription site, likely reflecting episodic polymerase release. Transcription then ceased after 40-50 minutes, with slightly less synchrony than at the onset ($\sim$ 20 min, Fig. 1**E**). *m5/m8* and *sim* thus direct transcription profiles that are highly co-ordinated temporally, with each conferring a prolonged period of activity that is initiated within a short time-window. Indeed, the mean profile of all the MSE cells was almost identical for the two enhancers (Fig. 1**F**). This is remarkable given they contain different configurations of binding motifs and implies that the mesectoderm cells undergo a highly synchronized period and level of Notch signaling. However, this profile is not a general property of Notch responsive enhancers, as a neuroectodermal enhancer of *E(spl)m8-bHLH* (*m8NE*, Fig. 1**A**) exhibits delayed and stochastic activity in the MSE compared to *m5/m8* and

sim (Fig. S1**AB**).

We next tested the consequences from substituting different promoters with the *m5/m8* and *sim* enhancers, to assess the relative contributions of the enhancer and promoter to the response profiles. First, when *peve* was replaced by a promoter from *sim* (*psimE*), both *m5/m8* and *sim* produced lower levels of transcription, but their overall temporal profiles remained similar and the mean levels were the same for the two enhancers (Fig. S1**C**). Second, we combined *m5/m8* with another heterologous promoter, *hsp70*, and with four promoters from the *E(spl)-C* genes that could be interacting with *m5/m8* in the endogenous locus. Similar to *psimE*, substituting these promoters also led to changes in the mean levels of transcription without affecting the overall temporal profile or expression pattern (Fig. S1**D**). Notably, even in combinations where the overall levels were lower, the transcription profiles remained sustained rather than breaking down into discrete bursts (Fig. S1**E**). Of those tested, *pm6* produced the lowest mean levels when combined with *m5/m8* (Fig. S1**D**). This is consistent with the fact that *E(spl)m6-BFM* is not normally expressed in the MSE and argues for an underlying enhancer-promoter compatibility at the sequence level (Fig. S1**D**) [51]. Nevertheless, the fact that similar temporal profiles were produced with all the promoters confirms that the enhancers are the primary detectors of Notch signaling activity.

To verify that transcription was indeed Notch-dependent we measured transcription from *m5/m8* in embryos where Notch activity was disrupted by mutations. In agreement, embryos lacking Neuralized, an E3 ubiquitin ligase required for Delta endocytosis that is critical for Notch signalling [18, 38], had no detectable transcription from *m5/m8* in the MSE (Fig. 1**G**). Likewise, *m5/m8* activity was severely compromised in embryos carrying mutations in *Delta*. Because Delta protein is deposited in the egg maternally [28], these embryos contained some residual Delta which was sufficient for a few scattered cells in the MSE stripe to initiate transcription (Fig. S1**F**). However their transcription ceased prematurely, within <20 min (Fig. 1**G**, S1**F**). Together these results confirm that the enhancers require Notch signalling for their activity, in agreement with previous studies of these regulatory regions [39], and further show that sustained Notch signalling is needed to maintain transcription, arguing that the enhancers are also detecting persistence of the Notch signal.

Coordinated activity of enhancers within each nucleus

Although *m5/m8* and *sim* confer well coordinated temporal profiles of transcriptional activity, there is nevertheless some cell to cell variability in the precise time of their activation. To investigate whether this cell to cell variability was due to the stochastic nature of transcription (intrinsic variability) or whether it indeed reflects changes in signalling from Notch (extrinsic variability) we monitored expression from two identical alleles of the MS2 reporters, supplied by the paternal and maternal chromosomes (Fig. 2**A**). Transcription from these two physically

unlinked loci were detected as distinct puncta in each nucleus so could be tracked independently. We found a remarkable synchrony in the onset of transcription from both alleles of a given enhancer (Fig. 2**B**, more than 80% of the cells initiated transcription from both alleles less than 5 min apart, Fig. S2**C**), indicating that most of the temporal variability in transcription onset between cells was due to extrinsic factors. There was less synchrony between the two alleles in the time at which transcription was extinguished (Fig. 2**B** S2**A**), but the extent of variability was much lower than that between cells (only contributing to less than 15% of the total variability, Fig. 2**D**) and it likely occurs because there will be locus to locus variations in the stage of the transcription cycle when the signaling levels decline.

Although the overall temporal profiles of transcription from the two alleles were similar to one another, in terms of the onset and overall increases or decreases in levels, the fine grained spikes and troughs were not synchronised (Fig. 2**A**), in agreement with the expectation that transcription from two different loci is largely uncorrelated [20, 27, 34]. However, the fluorescent intensities of two alleles are any time point displayed a small but significant positive correlation ($R^2 \sim 0.35$), compared to a null correlation when these pairs are randomly assigned (Fig. S2**B**). This argues that the enhancers at the two alleles operate independently while being co-ordinated by the same extrinsic signal information, namely the durations and levels of Notch activity. Even when the *m5/m8* and *sim* enhancers were placed in trans in the same cell, there was comparatively little variation in the onset times, compared to the variation in the onset of the enhancers in different cells (Fig. 2**CD** S2**A**). These results indicate that *m5/m8* and *sim* are reliably detecting extrinsic information in the form of Notch activity, which is initiated in the mesectoderm cells within a 5-10 minute time-window, so that within a given nucleus their activation is remarkably synchronized.

Enhancers detect signal thresholds and signal context

The *m5/m8* and *sim* enhancers appear to act as "persistence detectors", driving transcription as long as Notch signal(s) are present. They may therefore be simple "on-off" devices detecting when a signal crosses a threshold (digital encoding). Alternatively, the enhancers may have the capability to respond in a dose-sensitive manner to the levels of Notch activity (analog encoding). To distinguish these possibilities, we tested the consequences from additional Notch activity, in the form of the intracellular domain of the Notch receptor (NICD) supplied using the *stripe 2* regulatory enhancer from the *even-skipped* gene (*eve2-NICD*). This confers a tightly regulated ectopic stripe of NICD which is orthogonal to the MSE (Fig. 3**A**) [16, 29] and was sufficient to produce ectopic expression from both *m5/m8* and *sim* driven reporters (**Movie 3.**).

Whereas expression from *m5/m8* and *sim* was almost identical in wild-type embryos, clear differences in

their behaviour were revealed by ectopic NICD. First, transcription from *m5/m8* was detected throughout much of the region corresponding to the *eve2* stripe whereas transcription from *sim* was only seen in nuclei closest to the MSE (Fig. 3**B**), consistent with previous observations [16, 52]. Second, although both enhancers initiated transcription prematurely, because the ectopic NICD was produced from early nc14 [9], the onset of transcription from *m5/m8* was significantly earlier than that from *sim* (Fig. 3**DE**). Given that both enhancers are exposed to the same temporal pattern of NICD production, this difference in their initiation times implies that the two enhancers have different thresholds of response to NICD, with *m5/m8* responding to lower doses and hence being switched-on earlier. This is unexpected because *m5/m8* and *sim* responded at the same time in wild-type embryos and we hypothesize that this is because the normal ligand-induced signaling leads to a sharp increase in NICD. Importantly, the live analysis uncovers novel aspects of the enhancer sensitivity.

We also detected differences in the dynamics of *m5/m8* according to the location of the NICD-expressing nucleus along the DV axis. Nuclei closer to the MSE stripe (in the neuroectoderm, NE) exhibited strong activity, with a temporal pattern that resembled that in the MSE (Fig. 3**C**, bottom). In contrast nuclei in dorsal regions (dorsal ectoderm, DE) underwent resolved bursts of transcriptional activity (Fig. 3**C**, top). Ectopic NICD also induced 'bursty' expression from *sim* in the mesoderm (ME) (but was not capable of turning on *m5/m8* in that region). The positional differences in dynamics suggest that intrinsic cellular conditions, likely the expression levels of specific transcription factors, influence the way that enhancers "read" the presence of NICD. Such factors must therefore have the capability to modulate the dynamics of transcription.

The fact that *m5/m8* and *sim* are switched on at different times in the presence of ectopic NICD suggests that they require different thresholds for their activation. In addition, they only give sustained transcription profiles in a 2-3 cell-wide region overlapping the MSE, whereas elsewhere they generate stochastic and "bursty" transcription, arguing that they must be differently primed in the MSE region.

Notch activity tunes transcription burst size

To further test how Notch responsive enhancers respond to different doses of signal, we introduced a second *eve2-NICD* transgene. MSE transcription from *sim* in the presence of 2x*eve2-NICD* initiated earlier and achieved higher levels than with 1x*eve2-NICD* (Fig. 4**A**, left). This is consistent with the hypothesis that the *sim* enhancer responds to thresholds of NICD concentration, as the cells will reach a given concentration of signal more quickly in the embryos with 2x*eve2-NICD*. The mean levels of transcription increased in the ME as well as in the MSE regions (Fig. 4**AC**), further indicating a dose-sensitive response. In contrast, MSE transcription from *m5/m8* did not significantly change in 2x*eve2-NICD* embryos (Fig. 4**A**, right), arguing that the *m5/m8* enhancer reaches a

saturation point with the dose produced by 1x*eve2-NICD*. This only occurs in the MSE, as the more stochastic activity in the DE remains sensitive to increases in NICD, becoming responsive in a greater proportion of cells and remaining active over longer periods (Fig. S4**A**).

To distinguish different models for how NICD confers a dose-sensitive response, for example whether it is regulating enhancer activation or polymerase release, we took two strategies. Both approaches assume a two state model where the promoter is switched between an OFF and ON state with switching constants *Kon* and *Koff* to confer transcription initiation rate r in the ON state [33, 43]. In the first approach we used the macroscopic parameters of bursting amplitude, off period between bursts and bursting length as measures for r, *Kon* and *Koff*, respectively (Fig. 4**E**). In most previous enhancers analyzed in this way, the off period is the most affected, leading to changes in the frequency of bursting [20, 21, 31]. However, when we quantified the effect from different doses of NICD on *sim* in the ME, a region where individual bursts of transcription could be distinguished, we found that the bursting length consistently increased with higher amounts of NICD whereas the off period between bursts remained constant (Fig. 4**DF**). This indicates that the main effect of NICD is to keep the enhancer in the ON state for longer - ie. decreasing *Koff* - rather than increasing the frequency with which it becomes active (i.e. increasing *Kon*). The bursting amplitude also increased with 1x*eve2-NICD* but this was not further enhanced by 2x*eve2-NICD* (Fig. 4**DF**). Overall therefore, increasing levels of NICD in the ME result in *sim* producing an increase in transcription burst size (duration + amplitude) rather than an increase in the frequency of bursts. Transcription in other regions and enhancers (*m5/m8* DE and *m8NE* ME) showed similar increase in burst size in response to the dose of NICD (Fig. S4**A**-**C**) suggesting this is a general property of these Notch responsive enhancers.

We developed a second approach to analyze the changes in the dynamics where single bursts of activity could not be defined. To do so, we used a mathematical model of transcription to account for the initiating mRNA molecules (Fig. S3**A**). Using derivations from the mathematical model and testing them in simulations, we looked for the signatures that would be produced if the mean of initiating mRNAs (equivalent to the mean fluorescence from the MS2 puncta) were increasing due to changes in r, *Kon* or *Koff*. This showed that the effects on the Fano Factor ratio between the two conditions and on their autocorrelation function (ACF) could be used to correctly predict which of the three parameters could account for the increase in the mean (Fig. S3**B**, Methods). First we tested the modelling approach with the data from the promoter swap experiments. Analyzing the differences in the mean indicated that they are most likely due to increases in r (Fig. S3**F**), as expected if promoters influence the rate of polymerase release but not the activation of the enhancer per se. When we then applied the model to the data from the transcription profiles produced by different doses of NICD in the ME the results were most compatible with the causal effect being a decrease in *Koff* (Fig. S3**G**), i.e. this approach also indicated that NICD

elicits an increase in burst on-duration rather than in burst frequency. Thus the two approaches both converged on the model that, above the critical threshold level of NICD, further increases in NICD levels prolong the period that each enhancer remains in the ON state.

Finally, we then used an enhancer - promoter combination that produces higher mean levels (*m5/m8-pm5*, Fig. S1**D**) to investigate whether the saturation that occurred with ectopic NICD was due to the *peve* promoter having achieved a maximal initiation rate. Strikingly, the substitution of *pm5* did not result in significantly higher maximal levels than *m5/m8-peve* in the presence of *eve2-NICD* (Fig. S4**D**) although it did in wild-type signaling conditions (Fig. S1**D**). This result indicates that the saturation of the *m5/m8* response that occurs with higher levels of NICD stems from the *m5/m8* enhancer rather than the promoter and argues that enhancers reach a maximal "ON" state that they cannot exceed even if more NICD is provided.

Paired CSL motifs augment burst-size not threshold detection

The *m5/m8* and *sim* enhancers both respond to NICD but have different thresholds of response. How is this encoded in their DNA sequence? A prominent difference between the two enhancers is that *m5/m8* contains a paired CSL motif (so-called SPS motifs), a specific arrangement and spacing of binding motifs that permit dimerization between complexes containing NICD [40], whereas *sim* does not (Fig, S5**A**). To test their role, we replaced two of the CSL motifs in *sim* with the SPS motif from *m5/m8* and conversely perturbed the SPS in *m5/m8* by increasing the spacing between the two CSL motifs (Fig. S5**A**). As SPS motifs permit co-operative binding between two NICD complexes, we expected that enhancers containing an SPS motif (sim^{SPS} and *m5/m8*) would exhibit earlier onsets of activity than their cognates without (*sim* and $m5/m8^{insSPS}$). However this was not the case for either *sim* and sim^{SPS} (Fig. 5**AB**) or *m5/m8* and $m5/m8^{insSPS}$ in either wild type or *eve2-NICD* embryos (Fig. S5**DE**). These profiles suggest that the SPS motifs are not responsible for the difference in the threshold levels of NICD required for *m5/m8* and *sim* activation.

Changes to the CSL motifs did however affect the mean levels of activity. sim^{SPS} directed higher mean levels of activity compared to *sim* in both wild type and *eve-NICD* embryos (Fig. 5**A** S5**B**). Conversely, $m5/m8^{insSPS}$ directed lower levels compared to *m5/m8* (Fig. S5**D**). Analysing the traces from *sim* enhancer in the ME, where cells undergo bursts of transcription, revealed that the SPS site (sim^{SPS}) led to larger burst-sizes - i.e. increased the amplitude and the duration - compared to the native enhancer without SPS sites (*sim*) (Fig. 5**CD**). Conversely, the continuous profile produced by *m5/m8* in the MSE was broken into smaller bursts when the SPS was disrupted (Fig. S5**FG**). The effects on the bursting size are similar to those seen when the dose of NICD was altered, suggesting that enhancers containing SPS sites transmit a given level of NICD more effectively to the

initiation machinery. They do not however appear to affect the amount of NICD required for their initial activation, i.e. the threshold required for the enhancer to be switched on. This implies that the burst-size modulation and response threshold can be uncoupled and potentially could be encoded independently at the DNA level.

Regional factors prime enhancers for fast and sustained activation

Under ectopic NICD conditions, *m5/m8* and *sim* both produce sustained transcription profiles in the region overlapping the MSE and NE, whereas elsewhere they generate stochastic and "bursty" transcription. This suggests that other factors are "priming" the enhancers to respond to NICD. Good candidates are the factors involved in DV patterning at this stage, the bHLH transcription factor Twist (Twi) and/or the Rel protein Dorsal (dl). Indeed, the region where the enhancers generate sustained profiles in response to *eve2-NICD* coincides with the domain of endogenous Twist and Dorsal gradients (Fig S6**B**) [53]. Furthermore, *m5/m8* and *sim* both contain Twist and Dorsal binding motifs (Fig. S6**A**) and previous studies indicated that Twist is important for activity of *sim* although it was not thought to contribute to the activity of *m5/m8* [52].

To test if Twist and Dorsal are responsible for the different dynamics of transcription observed in *m5/m8* we mutated Twist and/or Dorsal binding motifs in *m5/m8*, which normally exhibits strong activity in the MSE and NE and a 'bursty' pattern in DE cells in conditions of ectopic Notch activity (Fig. 3**B**). Strikingly, mutation of either the three Twist motifs in *m5/m8* or the two Dorsal motifs produced a delay in the start of transcription in both WT and *eve2-NICD* embryos. These effects were even more pronounced when both Twist and Dorsal motifs were mutated together (Fig. 6**AB**), implying that, without Twist or Dorsal, *m5/m8* requires a higher threshold of NICD to become active. The mean transcription levels were also reduced in all cases (Fig. 6**A**).

Mutating the Twist motifs had two additional effects: the overall proportion of active cells in the MSE was reduced (Fig. 6**C**) and out of those active, fewer exhibited the sustained profile observed with the native enhancers (Fig. 6**DE**). Instead most cells displayed a 'bursty' transcription profile (Fig. 6**D**), similar to those elicited by NICD in the DE region. Although the mutated Twist motifs led to bursty profiles in wild type embryos, these effects were partially rescued when ectopic NICD was provided (Fig. 6**CE**). However, when both Dorsal and Twist motifs were mutated, the proportions of active cells and of cells with a sustained profile were both decreased even in the presence of ectopic NICD (although mutation of Dorsal motifs alone did not produce a significant decrease in either property) (Fig. 6**CE**). The results are therefore consistent with a role for Twist and Dorsal in priming the *m5/m8* enhancer to produce sustained activity. In their absence the ability of the enhancer to switch ON becomes much more stochastic. Consistently, another Notch responsive enhancer that only contains one Twist motif (the neuroectodermal enhancer *m8NE*, Fig. S6**A**) also exhibited a delayed onset of activity (Fig. S6**D**) and gave

stochastic bursting patters (Fig. 6**E**). This suggest that the two MSE enhancers are especially primed to respond in a fast and sustained manner at this stage.

Discussion

Developmental signaling pathways have widespread roles but currently we know relatively little about how the signaling information is decoded to generate the right transcriptional outcomes. We therefore set out to investigate the principles that govern how Notch activity is read by target enhancers in the living animal, using the MS2/MCP system to visualize nascent transcripts in *Drosophila* embryos and focusing on two enhancers that respond to Notch activity in the MSE. Three striking characteristics emerge. First, the MSE enhancers are sensitive to changes in the levels of NICD, which modulate the transcriptional burst size rather than increasing burst frequency. Second, the activation of both MSE enhancers is highly synchronous. Indeed, within one nucleus the two enhancers become activated within a few minutes of one another. Third, both MSE enhancers confer a sustained response in the wild-type context. This synchronized and persistent activity of the MSE enhancers is in stark contrast to the highly stochastic and bursty profiles that are characteristics of most other enhancers that have been analyzed [20, 21, 34] and relies on the MSE enhancers being "primed" by regional transcription factors Twist and Dorsal. We propose that such priming mechanisms are likely to be of general importance for rendering enhancers sensitive to signals so that a rapid and robust transcriptional response is generated.

Priming of enhancers sensitizes the response to NICD

Transcription of most genes in animal cells occurs in bursts interspersed with refractory periods of varying lengths, that are thought to reflect the kinetic interactions of the enhancer and promoter [3]. However, the MSE enhancers maintain transcription for 40-60 minutes, without any periods of inactivity. Calculation of the autocorrelation function in the traces from these nuclei suggest very slow transcriptional dynamics (Fig. S3**EF**) [19], which would be consistent with one long period of activity as opposed to overlapping short bursts. This fits with a model where promoters can exist in a permissive active state, during which many "convoys" of polymerase can be fired without the promoter reverting to a fully inactive condition [47]. The rapid successions of initiation events are thought to require Mediator complex [47], which was also found to play a role in the NICD-mediated increase in residence time of CSL complexes [26]. We propose therefore that the sustained transcription from *m5/m8* and *sim* reflects a switch into a promoter permissive state, in which general transcription factors like Mediator remain associated with the promoter so long as sufficient NICD is present, allowing repeated re-initiation.

However, the ability to drive fast and sustained activation is not a property of NICD itself. For example,

when ectopic NICD was supplied, cells in many regions of the embryo responded asynchronously and underwent only short bursts of activity. Furthermore, variable and less sustained cell-by-cell profiles were generated in the MSE region when the binding motifs for Twist and Dorsal in the *m5/m8* enhancer were mutated. The presence of these regional factors therefore appears to sensitize the enhancers to NICD, a process we refer to as enhancer priming. This has two consequences. First, it enables all nuclei to respond rapidly to initiate transcription in a highly coordinated manner once NICD reaches the threshold level. Second, it creates an effective 'state transition' so that the presence of NICD can switch the promoter into a permissive condition to produce sustained activity (Fig. 7).

Our explanation that the synchronous activation of the MSE enhancers reflects their requirements for a critical concentration of NICD is borne out by their responses when the levels of NICD are increased. Notably, while *sim* and *m5/m8* exhibited almost identical dynamics in wild-type embryos, they displayed clear differences in the presence of ectopic NICD, suggesting that they detect slightly different thresholds. Indeed, doubling the dose of ectopic NICD further accelerated the onset times of *sim* in agreement with the model that the enhancers detect NICD levels. Threshold detection does not appear to rely on the arrangement of CSL motifs, as the onset times of *m5/m8* or *sim* were unaffected by changes in the spacing of CSL paired sites. In contrast, mutating Twist or Dorsal binding-motifs in *m5/m8* delayed the onset of transcription, arguing that these factors normally sensitize the enhancer to NICD enabling responses at lower thresholds.

We propose that enhancer priming will be widely deployed in contexts where a rapid and consistent transcriptional response to signaling is important, as in the MSE where a stripe of cells with a specific identity is established in a short time-window. In other processes where responses to Notch are more stochastic, as during lateral inhibition, individual enhancers could be preset to confer different transcription dynamics. This appears to be the case for a second enhancer from *E(spl)-C* (*m8NE*) which generates a stochastic response in the MSE cells, similar to that seen for the MSE enhancers when Twist and Dorsal sites are mutated. This illustrates that the presence or absence of other factors can toggle an enhancer between conferring a stochastic or deterministic response to signalling.

NICD regulates transcription burst size

Manipulating the levels of NICD revealed that it has a consistent effect on enhancer activity irrespective of their priming state. This can be most readily quantified in regions where NICD elicits discrete bursts of transcription initiation, such as the dorsal ectoderm for *m5/m8* or mesoderm for *sim* and *m8NE*. Transcriptional bursting has been formalized as a two-state model where the promoter toggles between on and off states, conferring a

transcription initiation rate [33, 43]. Changes in the duration or frequency of the bursts lead to an overall increase in transcription. Most commonly, differences in the activity of enhancers have been attributed to changes in the probability of the enhancer switching on (K_{on}) which produce different off periods between bursts, leading to changes in burst frequency [4, 20, 21, 31, 32, 46]. Unexpectedly, higher doses of NICD do not increase the burst frequency. Instead they produce bigger bursts, both by increasing the bursting amplitude, equivalent to the rate of transcription initiation, and the bursting length, indicative of the total time the enhancer stays in the on state. Modifications to the CSL motifs also impact on the same parameters. Thus, enhancers with paired motifs (SPS), which favour NICD dimerization [40], produce larger transcription bursts than those where the motifs are further apart. This suggests that paired motifs can 'use' the NICD present more efficiently. Interestingly, even though *m5/m8* and *sim* contain different arrangements and numbers of CSL motifs they have converged to produce the same mean levels of transcription in wild type embryos.

Two models would be compatible with the observations that effective NICD levels alter the burst size. In the first model, increasing the concentration of NICD when the enhancer is activated would create larger Pol II clusters. This is based on the observation that low complexity activation domains in transcription factors can form local regions of high concentration, so-called "hubs", which in turn are able to recruit Pol II [35, 36, 48]. As the lifetime of Pol II clusters appears to correlate with transcriptional output [13], the formation of larger Pol II clusters would in turn drive larger bursts. In the second model, NICD would be required to keep the enhancer in the ON state, for example by nucleating recruitment of Mediator and/or stabilizing a loop between enhancer and promoter, which would in turn recruit Pol II in a more stochastic manner. General factors such as Mediator have been shown to coalesce into phase-separated condensates that compartmentalize the transcription apparatus [7, 14, 45] and these could form in an NICD dependant manner. Whichever the mechanism, the clusters/ON state must persist in a state that requires NICD yet is compatible with NICD having a short-lived interaction with its target enhancers [26]. Furthermore, the fact that the activity of *m5/m8* enhancer saturates with one *eve2-NICD* construct, and can't be enhanced by providing a more active promoter, suggests that that there is a limit to the size or valency of the clusters that can form.

Although unexpected, the ability to increase burst size appears to be a conserved property of NICD. Live imaging of transcription in response to the Notch homologue, GLP1, in the *C.elegans* gonad also shows a change in burst size depending on the signalling levels. As the capability to modulate burst size is likely to rely on the additional factors recruited, the similarities between the effects in fly and worm argue that a common set of core players will be deployed by NICD to bring about the concentration-dependant bursting properties.

Materials and Methods

Cloning and transgenesis

Generation of MS2 reporter constructs

MS2 loops were placed upstream of a lacZ transcript and both were driven using different combinations of enhancers and promoters. 24 MS2 loops were cloned from *pCR4-24XMS2SL-stable* (Addgene #31865) into pLacZ2-attB [5] using *Eco*RI sites. The *m5/m8*, *sim* and *m8NE* enhancers [30, 52] were amplified from genomic DNA and cloned into *pattB-MS2-LacZ* using *Hin*dIII/*Age*I sites (primers in Table **??**). Subsequently the promoters *hsp70*, *peve*, *pm5*, *pm6*, *pm7*, *pm8* and *psimE* were cloned by Gibson Assembly [23] in *pattB-m5/m8-MS2-LacZ*, *pattB-sim-MS2-LacZ* and/or *pattB-m8NE-MS2-LacZ* (primers in Table 1) using the *Age*I restriction site and incorporating a *Eag*I site. All mutations introduced in *m5/m8* or *sim* were first introduced by Gibson Assembly in the enhancers contained in pCR4 plasmids and then transferred to *pattB-peve-MS2-lacZ* using *Hin*dIII and *Age*I sites.

Su(H), Twi, dl and sna binding motifs were identified using ClusterDraw2 using the PWM from Jaspar for each transcription factor. Motifs with scores higher than 6 and pvalues < 0.001 were selected.

Primers to create sim^{SPS}, $m5/m8^{insSPS}$, $m5/m8^{\Delta twi}$, $m5/m8^{\Delta dl}$ and $m5/m8^{\Delta twi\ \Delta dl}$ are detailed in Table **??**.

The following constructs have been generated and inserted by ΦC31 mediated integration [6] into an *attP* landing site in the second chromosome – *attP40*, 25C – to avoid positional effects in the comparisons: *pattB-m5/m8-peve-MS2-LacZ*, *pattB-m5/m8-hsp70-MS2-LacZ*, *pattB-m5/m8-pm5-MS2-LacZ*, *pattB-m5/m8-pm6-MS2-LacZ*, *pattB-m5/m8-pm7-MS2-LacZ*, *pattB-m5/m8-pm8-MS2-LacZ*, *pattB-m5/m8-psimE-MS2-LacZ*, *pattB-sim-peve-MS2-LacZ*, *pattB-sim-psimE-MS2-LacZ*, *pattB-*sim^{SPS}*-peve-MS2-LacZ*, *pattB-*$m5/m8^{insSPS}$*-peve-MS2-LacZ*, *pattB-*$m5/m8^{\Delta twi}$*-peve-MS2-LacZ*, *pattB-*$m5/m8^{\Delta dl}$*-peve-MS2-LacZ* and *pattB-*$m5/m8^{\Delta twi\ \Delta dl}$*-peve-MS2-LacZ*.

Expression of ectopic NICD

To generate *eve2-NICD* the plasmid 22FPE [29], which contains 2 copies of the *eve2* enhancer with five high affinity *bicoid* sites, FRT sites flanking a transcription termination sequence and the *eve 3'UTR*, was transferred to *pGEM-t-easy* using *Eco*RI sites and from there to *pattB* [5] using a *Not*I site. The NICD fragment from Notch was excised from an existing *pMT-NICD* plasmid and inserted in *pattB-22FPE* through the *Pme*I site to create the *pattB-eve2x2-peve-FRT-STOP-FRT-NICD-eve3'UTR* construct (referred as *eve2-NICD*). This was inserted into the *attP* landing site at 51D in the second chromosome. To increase the amount of ectopic NICD produced, the

same *eve2-NICD* construct was also inserted in the *attP40* landing site at 25C and recombined with *eve2-NICD*51D to produce 2x*eve2-NICD*.

Fly strains and genetics

To observe the expression pattern and dynamics from *m5/m8-peve*, *sim-peve* and the different promoter combinations (Fig. 1, S1) females expressing His2av-RFP and MCP-GFP (BDSC #60340) in the maternal germline were crossed with males expressing the MS2-lacZ reporter constructs.

To test expression from *m5/m8-peve* in the *Dl* and *neur* mutant backgrounds, *His2Av-RFP* from *His2av-RFP ; nos-MCP-GFP* (BDSC #60340) was recombined with *nos-MCP-GFP* in the second chromosome (BDSC #63821) and combined with a deficiency encompasing the *Dl* gene (*Df(3R)Dl*^{FX3}, [49]) or a *neuralized* loss of function allele (*neur*$^{[11]}$, BDSC #2747). *m5/m8-peve-MS2-lacZ* was also combined with the *Dl* and *neur* alleles and mutant embryos were obtained from the cross *His2Av-RFP,nos-MCP-GFP ; mut / TTG* x *m5/m8-peve-MS2-lacZ ; mut / TTG*. Homozygous mutant embryos for *Dl* or *neur* were selected by the lack of expression from the *TTG* balancer (*TM3-twi-GFP*).

To observe transcripion from two MS2 reporters in each cell (Fig. 2, S2) *His2Av-RFP* (BDSC #23650) was recombined with *nos-MCP-GFP* (from BDSC #60340) in the third chromosome and combined with *m5/m8-peve* or *sim-peve* MS2 reporters. *m5/m8-peve* x2 embryos and *sim-peve* x2 embryos were obtained from the stocks *m5/m8-peve-MS2-LacZ ; His2Av-RFP,nos-MCP-GFP* and *sim-peve-MS2-LacZ ; His2Av-RFP,nos-MCP-GFP*, respectively; while *m5/m8-peve + sim-peve* embryos were obtained from crosssing *sim-peve-MS2-LacZ ; His2Av-RFP,nos-MCP-GFP* females with *m5/m8-peve-MS2-LacZ* males.

To observe transcription from MS2 reporters in conditions of ectopic Notch activity the *FRT-STOP-FRT* cassette had to be first removed from the *eve2-NICD* construct by expression of a flippase in the germline. To do so flies containing *ovo-FLP* (BDSC #8727), *His2Av-RFP* and *nos-MCP-GFP* were crossed with others containing *eve2-FRT-STOP-FRT-NICD*, *His2Av-RFP* and *nos-MCP-GFP*. The offspring of this cross (*ovo-FLP/+ ; eve2-FRT-STOP-FRT-NICD/+ ; His2Av-RFP, nos-MCP-GFP*) induced FRT removal in the germline and were crossed with the MS2 reporters to obtain embryos expressing ectopic NICD. We note that only half of the embryos present the *eve2-NICD* chromosome, which could be distinguished by ectopic MS2 activity and an ectopic cell division of all the cells in the eve2 stripe after gastrulation. The other 50% embryos obtained from this cross were used as the wild type controls. This strategy was used to observe transcription from *m5/m8-peve*, *sim-peve*, *m8NE-peve*, *m5/m8-pm5*, *sim*^{SPS}*-peve*, *m5/m8*^{insSPS}*-peve*, *m5/m8*$^{\Delta twi}$*-peve*, *m5/m8*$^{\Delta dl}$*-peve* and *m5/m8*$^{\Delta twi\ \Delta dl}$*-peve*. To measure transcription from 2x*eve2-NICD* (Fig. 4, S4) removal of the *FRT-STOP-FRT*

cassete was induced from the male germline to avoid recombination. To do so, *betaTub85D-FLP* (BDSC #7196) females were crossed with 2x*eve2-NICD* males and the male offspring of this cross (*betaTub85D-FLP/Y ; 2xeve2-NICD/+*), which induces FRT removal in the germline, were crossed with *m5/m8-peve-MS2-lacZ ; His2AvRFP, nos-MCP-GFP* or *sim-peve-MS2-lacZ ; His2AvRFP, nos-MCP-GFP* females. As in the previous strategy, only half of the embryos presented the 2x*eve2-NICD* chromosome and were distinguished by the ectopic activity.

Live imaging

Embryos were dechorionated in bleach and mounted in Voltalef medium (Samaro) between a semi-permeable membrane and a coverslip. The ventral side of the embryo was facing the coverslip in all movies except when looking at transcription in the DE region (Fig. 3**B**, S4**AC**), in which they were mounted laterally. Movies were acquired in a Leica SP8 confocal using a 40x apochromatic 1.3 objective and the same settings for MCP-GFP detection: 40mW 488nm argon laser detected with a PMT detector, pinhole airy=4. Other settings were slightly different depending on the experiment. To observe transcription in the whole embryo (Fig. 1) settings were: 3% 561nm laser, 0.75x zoom, 800x400 pixels resolution (0.48um/pixel), 19 1um stacks, final temporal resolution of 10 seconds/frame). To observe transcription from 2 MS2 alleles simultaneously (Fig. 2) settings were: 2% 561nm laser, 1.5x zoom, 800x400 pixels resolution (0.24um/pixel), 29 1um stacks, final temporal resolution of 15s/frame). In all experiments with ectopic NICD a ∼150x150um window anterior to the center of the embryo was captured. Settings were: 2% 561nm laser, 2x zoom, 400x400 pixels resolution (0.36um/pixel), 29 1um stacks, final temporal resolution of 15s/frame). All images were collected at 400Hz scanning speed in 12 bits.

Image analysis

Movies were analyzed using custom Matlab (Matlab R2018a, Mathworks) scripts (available at). Briefly, the His2Av-RFP signal was used to segment and track the nuclei in 3D. Each 3D stack was first filtered using a median filter, increasing the contrast based on the profile of each frame to account for bleaching and a fourier transform log filter [22]. Segmentation was performed by applying a fixed intensity threshold, 3D watershed accounting for anisotropic voxel sizes [37] to split merged nuclei and thickening each segmented object. Nuclei were then tracked by finding the nearest object in the previous 2 frames which was closer than 6 um. If no object was found, that nuclei was kept with a new label, and only one new object was allowed to be tracked to an existing one. After tracking, the 3D shape of each nucleus in each frame was used to measure the maximum fluorescence value in the GFP channel, which was used as a proxy of the spot fluorescence. We note than when a spot cannot be

detected by eye this method detects only background, but the signal:background ratio is high enough that the subsequent analysis allows to classify confidently when the maximum value is really representing a spot.

In experiments with two MS2 reporters the maximum intensity pixel per nucleus does not allow to separate transcription from the two alleles. To do so, the 3D Gaussian spot detection method from [22] was implemented in the existing tracking, such that each spot was segmented independently and associated with the overlapping nuclei. In this manner only active transcription periods were detected and no further processing of the traces was required.

MS2 data processing

From the previous step we obtained the fluorescent trace of each nuclei over time. Only nuclei tracked for more than 10 frames were kept. First nuclei were classified as background or signal. To do so the average of all nuclei (background and signal) was calculated over time and fitted to a straight line. A median filter of 3 was applied to each nuclei over time to smooth the trace and ON periods were considered when fluorescent values were 1.2 times the baseline at each time point. This produced an initial classification of signal (nuclei ON for at least 5 frames) and background. Using these background nuclei, the mean fluorescence was fitted again to redefine the background baseline and background:signal nuclei were classified again. Nuclei were then classified as MSE or earlier stages and the MSE ones were kept for further analysis.

The final values for each nuclei (NormF) were calculated by removing the fitted baseline from the maximum intensity value for each and normalizing for the percentage that fluorescence in background nuclei decreases over time to account for the loss of fluorescence due to bleaching.

In all movies time into nc14 was considered from the end of the 13th syncythial division. When this was not captured they were synchronized by the gastrulation time.

Each nuclei was classified into the 4 regions (ME, MSE, NE and DE) by drawing rectangular shapes in a single frame and finding which centroids overlapped with each region. In *eve2-NICD* these regions along the DV axis were defined within the *eve2* stripe ($\sim$ 6-7 cells wide in all movies). In wild type embryos ME and MSE regions were drawn in the whole field of view ($\sim$ 150x150 um anterior half of the embryo).

Definition of bursting properties

Bursts were defined as periods were the median filtered signal was higher than 1.2 times the baseline for at least 5 frames after the initial burst of activity at the beginning of nc14 (the considererd period started at 15 min into nc14). These defined the burst duration and the time off between bursts. The amplitude was defined as the maximum value within each burst period. Onsets and ends of transcription were defined as the beginning of the

first burst and the end of the last respectively (also starting at 15 min into nc14). In Fig. 2 to be more precise in measuring the onsets and end-points of transcription for both MS2 alleles they were scored manually as the first and last frame a spot is detected and randomly assigned 'allele 1' or 'allele 2'. The total variability was the variance of all onsets or end points, combining both alleles. The extrinsic variability was calculated as the covariance of onsets and ends between alleles 1 and 2. The remaining (total - covariance) corresponds to the intrinsic variability within each cell.

Modelling changes in kinetic parameters of transcription

We developed a two-state promoter model of transcriptional activation in which the promoter switches between OFF and ON with constants K_{on} and K_{off} and releases mRNAs at a rate r when the promoter is ON (Fig.S3**E**). To be the most representative of what MS2 measures, ie. initiation events rather than overall levels of mRNA in the cell, the model does not include a degradation rate and instead accounts for the accumulation of initiation events. The mean and variance of the population at any time point can be defined by (**details on how to get here...**):

$$\langle m \rangle = \frac{r \cdot K_{on}}{K_{on} + K_{off}}\, dt$$

$$\sigma^2 = \frac{r \cdot K_{on}}{K_{on} + K_{off}} + \frac{2 \cdot r^2 \cdot K_{on} \cdot K_{off}}{(K_{on} + K_{off})^3}\, dt$$

Therefore the mean levels of transcription could increase in three ways: by increasing r, increasing K_{on} or decreasing K_{off}.

Aiming to infer underlaying changes in the mean, we decided to use the noise intrinsic to transcription - via measuring the Fano Factor - to test whether the same change in the mean could have different 'signatures' on the noise depending on which kinetic parameter was being modified.

$$FanoFactor = \frac{\sigma^2}{\langle m \rangle} = 1 + \frac{2 \cdot r \cdot K_{on}}{(K_{on} + K_{off})^2}$$

For each of the three possible modes of regulation we obtained how much each parameter had to change to produce a given change in the mean. We then used these to obtain the expected change in the Fano Factor. First we define α as the fold change in mean levels of transcription: $\langle m_2 \rangle = \alpha \cdot \langle m1 \rangle$, then:

$$\frac{r_2 \cdot K_{on2}}{K_{on2} + K_{off2}} = \alpha \cdot \frac{r_1 \cdot K_{on1}}{K_{on1} + K_{off1}}$$

if only r changes: $K_{on1} = K_{on2}$; $K_{off1} = K_{off2}$;

$$r_2 = \alpha \cdot r_1 \tag{1}$$

if only K_{on} changes: $r_1 = r_2$; $K_{off1} = K_{off2}$;

$$K_{on2} = \frac{K_{off1}}{\frac{K_{off1} + K_{on1}}{\alpha \cdot K_{on1}} - 1} \tag{2}$$

if only K_{off} changes: $r_1 = r_2$; $K_{on1} = K_{on2}$;

$$K_{off2} = \frac{(1-\alpha) \cdot K_{on1} + K_{off1}}{\alpha} \tag{3}$$

From the expressions for K_{on2} and K_{off2} when K_{on} increases (2) and K_{off} decreases (3), respectively, we note that given certain α, K_{on1} and K_{off1} values, the obtained K_{on2} and K_{off2} would be negative or infinite. From this we get the additional constrain that for K_{on2} and K_{off2} to be positive:

$$K_{off1} > (\alpha - 1) \cdot K_{on1}$$

Increasing the mean by increasing r doesn't have this additional constrain, as just according to the model r could increase to infinity. In reality there can't be more polymerases released than the space each of them takes on DNA. We calculated for an elongation rate of 2kb/min and if each polymerase takes 100bp of DNA then the maximum initiation rate r before the polymerases jam is $\sim 0.3s^{-1}$ (it'd take $\sim 3s$ for one polymerase to move enough that the next one can be released).

To see the effect that each of these possible modes of increasing the mean would have on the transcriptional noise we define the Fano Factor ratio:

$$FF = \frac{FF_{m2}}{FF_{m1}} = \frac{\frac{2 \cdot r_2 \cdot K_{off2}}{(K_{on2} + K_{off2})^2} + 1}{\frac{2 \cdot r_1 \cdot K_{off1}}{(K_{on1} + K_{off1})^2} + 1} \tag{4}$$

Substituting in (4) $r_2(1)$, $K_{on2}(2)$ or $K_{off2}(3)$ we obtain for each possibility:

if only r changes: all FFRatio values are greater than 1 (Fig. S3**D**, top panel).

$$FF_r(\alpha, r_1, K_{on1}, K_{off1}) = \frac{1 + \frac{2 \cdot \alpha \cdot K_{off1} \cdot r_1}{(K_{off1} + K_{on1})^2}}{1 + \frac{2 \cdot K_{off1} \cdot r_1}{(K_{off1} + K_{on1})^2}} \tag{5}$$

if only K_{on} changes: all allowed FFRatio values are smaller than 1 (Fig. S3**D**, middle panel).

$$FF_{Kon}(\alpha, r_1, K_{on1}, K_{off1}) = \frac{1 + \frac{2 \cdot r_1 \cdot (K_{off1} + K_{on1} - \alpha \cdot K_{on1})^2}{K_{off1}(K_{off1} + K_{on1})^2}}{1 + \frac{2 \cdot r_1 \cdot K_{off1}}{(K_{off1} + K_{on1})^2}} \tag{6}$$

if only K_{off} changes: allowed FFRatio values can be greater or smaller than 1 depending on the initial K_{on1} and K_{off1} values (Fig. S3**D**, bottom panel).

$$FF_{Koff}(\alpha, r_1, K_{on1}, K_{off1}) = \frac{K_{off1}^2 + 2 \cdot K_{off1}(K_{on1} + \alpha \cdot r_1) + alpha \cdot r_1 \cdot K_{on1}(K_{on1} - 2(\alpha - 1))}{K_{off1}^2 + K_{on1}^2 + 2K_{off1}(K_{on1} + r_1)} \tag{7}$$

We next tested with simulations whether the Fano Factor ratio can be used as a diagnostic tool of the underlying changes in the mean. We used stochastic simulations of transcription based on the Gillespie algorithm [24] of the same two-state promoter model but using additional parameters to resemble more the biological MS2 data (accounting for the time MS2 loops are detected, acquisition time and adding experimental noise). First we tested whether we could recover the same trends in Fano Factor ratios in the simulation as expected from the mathematical model. Indeed, using a variety of starting parameters we could recover similar Fano Factor values as expected from the mathematical model (Fig. S3**D**). However, given that changes in K_{off} can produce Fano Factor ratios greater or smaller than 1, calculation of the Fano Factor alone is not sufficient to infer which parameter is being modified to produce the observed changes in the mean.

As an additional measure to the Fano Factor ratio we used the autocorrelation function (ACF) to detect changes in the dynamics of transcription. The AC function provides information about the speed of the system (curved or pointy angles) and the elongation rate [19,31]. We used the same simulations to see if the autocorrelation function changes in different ways depending on the modified parameters to help distinguishing between the 3 ways to change the mean. If the dynamics are fast (Fig.S3**E**, right column) no changes in the ACF were observed in any of the three cases. When the dynamics are slower (Fig.S3**E**, left column), then the AC function shifts to the right when K_{off} decreases and in some cases shows a small shift to the left when K_{on} increases.

Therefore looking at both the Fano Factor ratio and the autocorrelation function (when the dynamics are slow enough), provides enough information to distinguish between the three ways in which the mean can change

(Fig. S3**B**).

When applied to biological data MS2 traces were processed by applying a median filter of 3, removing the background baseline and normalized for bleaching as previously described. When the onset of transcription was different between experiments (eg. WT vs *eve2-NICD*) they were shifted to compare equivalent times.

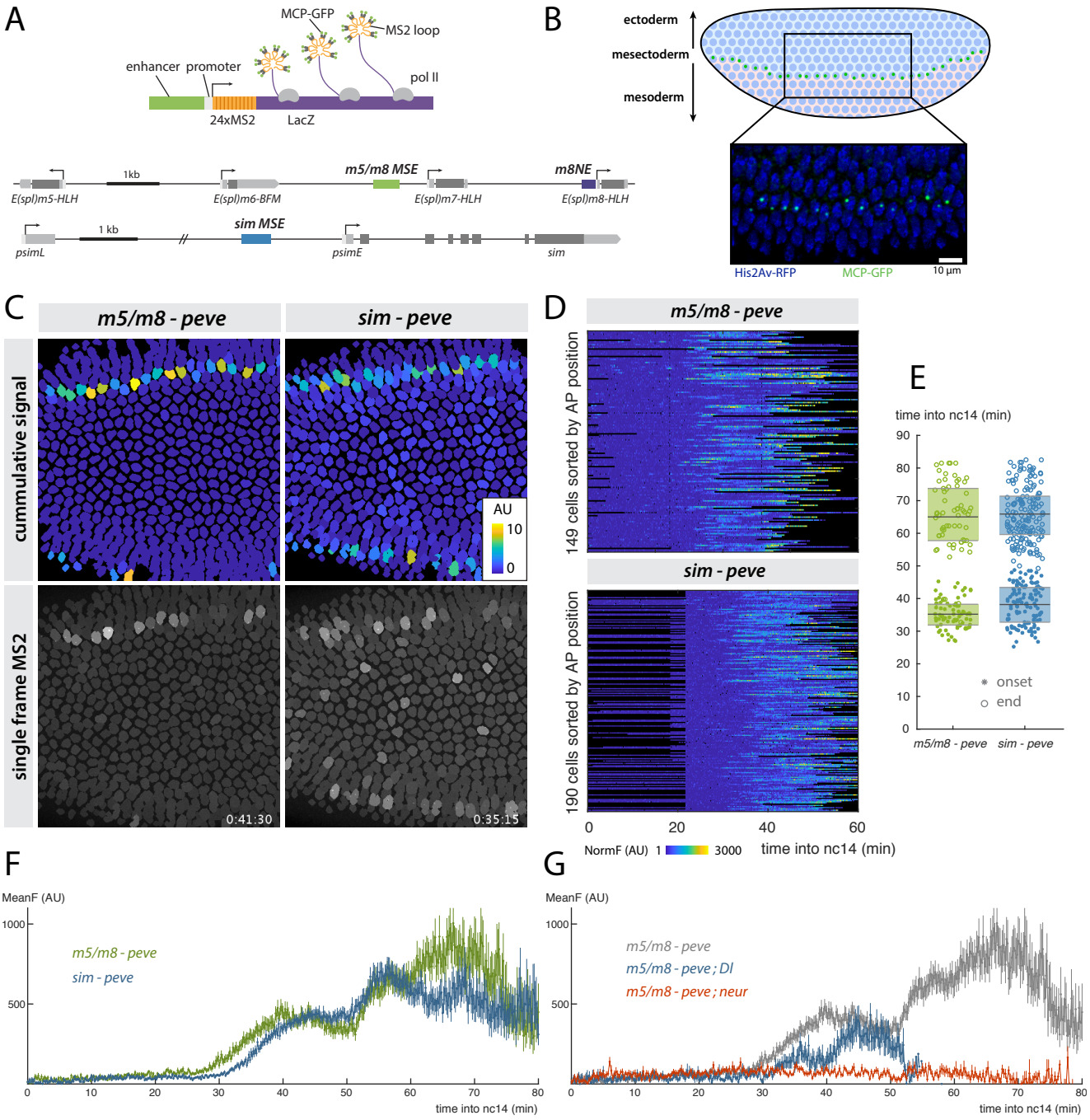

Figure 1. Synchronous activity of two Notch responsive enhancers. A) Diagrams illustrating the strategy for live imaging of transcription using the MS2 system (top) and the location of mesectoderm (MSE) and neuroectoderm (NE) enhancers from the *E(spl)*locus (*m5/m8*, green and *m8NE*, purple) and *single minded* gene (*sim*, blue) (bottom). Arrows indicate promoters/transcription start-sites and boxes in lower panel indicate non-coding (light grey) and coding (dark grey) transcribed regions. **B**) Diagram of a blastoderm *Drosophila* embryo, indicating region of Delta expression (pink) in the mesoderm which activates the Notch pathway in a flanking stripe of cells (green dots) to specify the MSE. Transcription from the *m5/m8* reporter is detected in each of the cells in the stripe by accumulation of MCP-GFP in bright puncta at the transcription site (see panel where nuclei are labelled by His2Av-RFP, blue). **C**) Tracked expression from *m5/m8* and *sim* reporters. Top panels: tracked nuclei are false-colored by their total signal levels, proportional to their total mRNA production, showing that both *m5/m8* and *sim* direct expression in 1-cell wide MSE stripes. Bottom panels: single frame of *m5/m8* and *sim* embryos. Tracked nuclei are shaded by their maximum pixel intensity in that frame. In addition to MSE cells, *sim* also exhibits low sporadic activity in some mesodermal cells. **D**) *m5/m8* and *sim* initiate transcription synchronously in all MSE cells. Heat-maps representing time-course during nc14 of all fluorescence traces from MSE cells in

Figure 1 (continued). *m5/m8* and *sim* embryos (scale as indicated where blue is no expression and yellow is high expression; black indicates periods where nuclei were not tracked). Transcription begins within 30-35 min into nc14. **E**) Onsets (solid circles) and end-point (open circles) of transcription from *m5/m8* (green) and *sim* (blue) in MSE cells. Transcription starts synchronously in a 10 minute window from 30 min into nc14 and is extinguished 30 to 60 min afterwards. Boxplots indicate mean, and 25/75 quartiles. **F**) *m5/m8* (green) and *sim* (blue) produce similar average temporal profiles. Mean fluorescent intensity of MCP-GFP puncta, (arbitrary units, AU) at the indicated times after start of nc14. **G**) Transcription from *m5/m8* is curtailed in embryos lacking zygotic production of Delta (Dl, blue) and abolished in embryos lacking neuralized (neur; red). Grey trace is profile from *m5/m8* in wild-type embryos shown in **F**. In **F** and **G** mean and SEM of all MSE cells are shown. n = 3 (*m5/m8*), 3 (*sim*), 2 (*m5/m8 ; Dl*), 2 (*m5/m8 ; neur*) embryos.

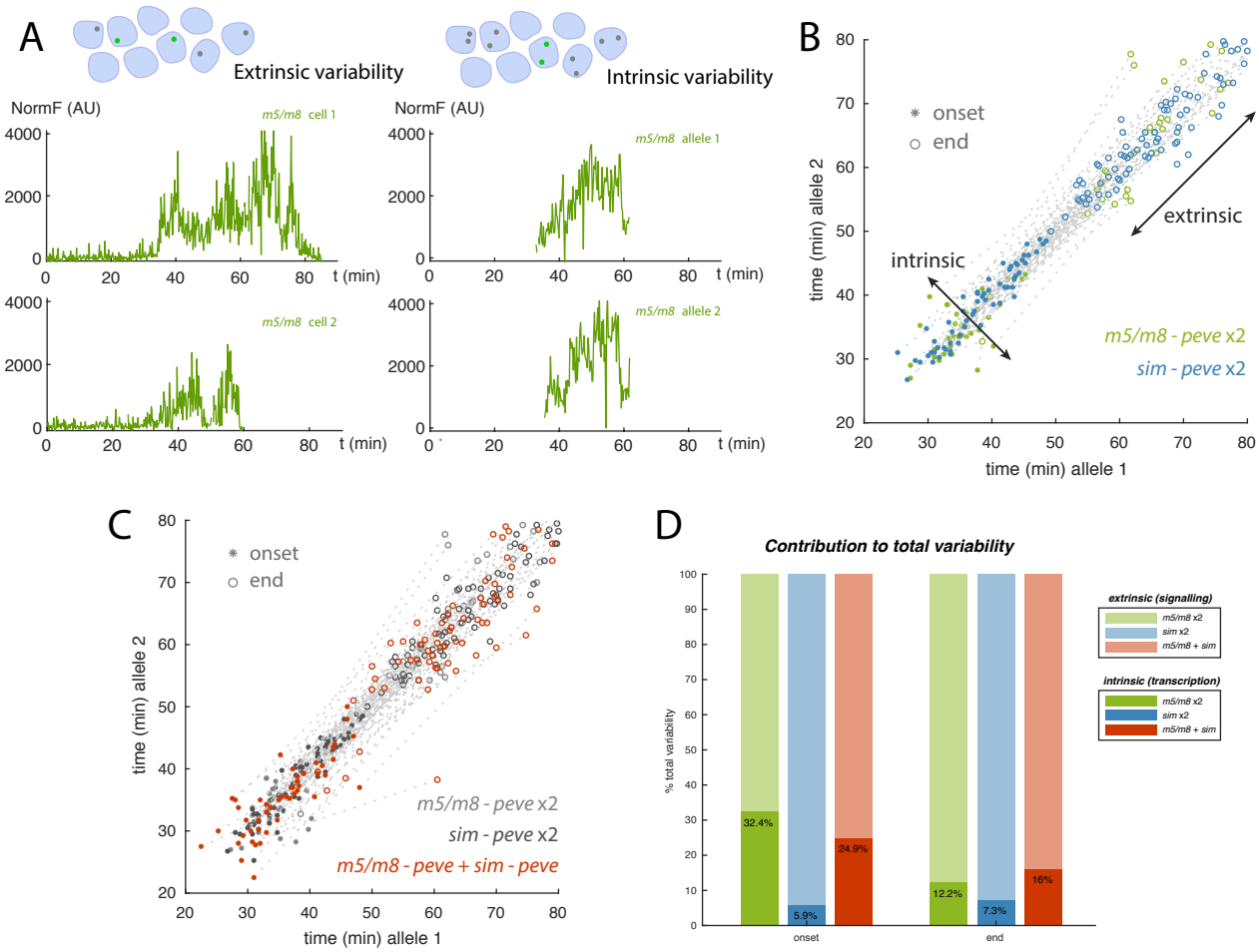

Figure 2. Notch enhancers exhibit low intrinsic variability. **A**) Examples of fluorescence traces from different cells (left panels) where variability is due to extrinsic effects (e.g. signaling). Examples of fluorescence traces from two alleles in the same cell (right panels) illustrating low intrinsic transcriptional variability between the enhancers. **B**) *m5/m8* and *sim* both exhibit low intrinsic variability in their onset and end-point of activity. Fluorescence intensity from individual puncta was quantified in nuclei carrying two alleles of *m5/m8* (green) or *sim* (blue) and their relative onset and end-point of activity plotted. Distribution across the diagonal reflects intrinsic variability (within cells) whereas distribution along the diagonal reflects extrinsic variability (between cells). **C**) *m5/m8* and *sim* exhibit highly correlated activity. Fluorescence intensity from individual puncta was quantified in nuclei carrying an allele of *m5/m8* and an allele of *sim* and their relative onset and end-points plotted (red) (with data from the individual enhancers, **C**, shown in grey for comparison). **D**) Variability intrinsic to transcription (dark shading) contributes a small percentage of the observed total variability in onsets and end-points of transcription from the MSE enhancers, in comparisons of two alleles, as indicated. In **B** and **C** onsets and ends are randomly assigned allele 1 or 2. Connecting grey lines indicates onset and end times come from the same cell. n = 2 (*m5/m8*x2), 3 (*sim*x2), 3 (*m5/m8* + *sim*) embryos.

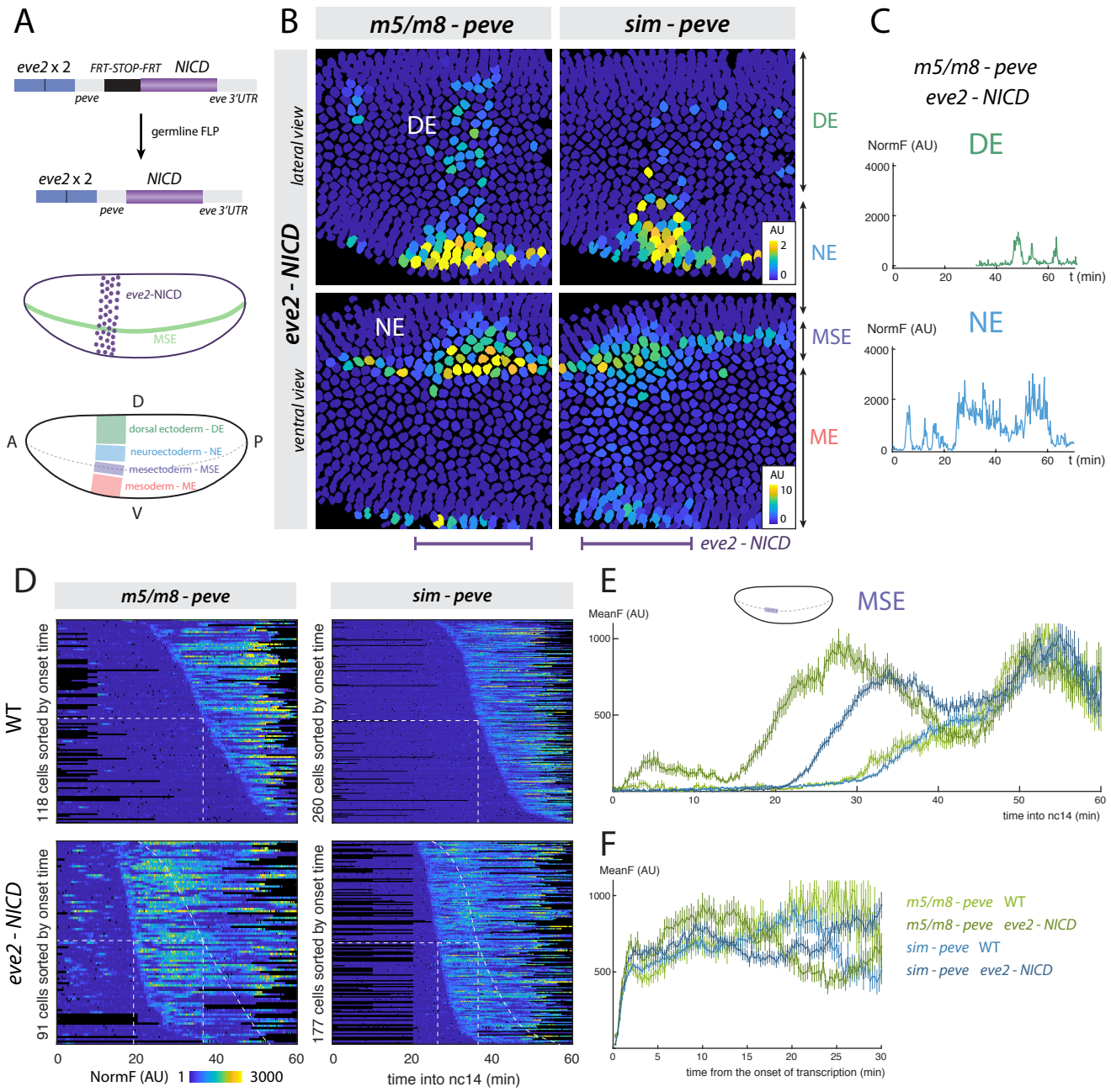

Figure 3. Effects of ectopic NICD on temporal transcription profiles reveals enhancers have different thresholds. A) Diagram illustrating the strategy for producing ectopic NICD in a stripe orthogonal to the MSE using the *eve stripe 2* enhancer (*eve2*), with schematic showing site of expression (purple shading) relative to the MSE stripe (green) and an overview of the regions along the DV axis where the effects on transcription were quantified. **B**) Still frames of tracked nuclei false-colored with the total accumulated signal (see scales). DE, NE, MSE, ME correspond to the regions shown in **A**. Both *m5/m8* and *sim* have strongest responses in NE/MSE region. *m5/m8* activity is also detected in sporadic dorsal ectoderm (DE) nuclei. Conversely *sim* exhibits low sporadic activity in mesodermal cells (ME). **C**) NICD produces different transcription profiles from *m5/m8* depending on DV cell context, illustrative traces from DE (top) and NE (bottom). **D**) Heatmaps of transcription traces from all MSE cells in *m5/m8* and *sim* in wild type and *eve2-NICD* embryos, sorted by onset time. Both enhancers are active earlier and more synchronously in *eve2-NICD*, with *m5/m8* shifted to a greater extent than *sim*. **E**) Mean profiles of activity in MSE nuclei, *m5/m8* and *sim* give earlier onsets and higher levels of transcription in *eve2-NICD*. **F**) Aligned onset times from all nuclei, mean transcription increases steeply in all conditions. More gradual mean increase, **E**, reflects the small differences in onset times between nuclei. **E** and **F** show mean and SEM of all MSE cells. n = 4 (*m5/m8* WT), 7 (*sim* WT), 6 (*m5/m8 eve2-NICD*), 8 (*sim eve2-NICD*) embryos.

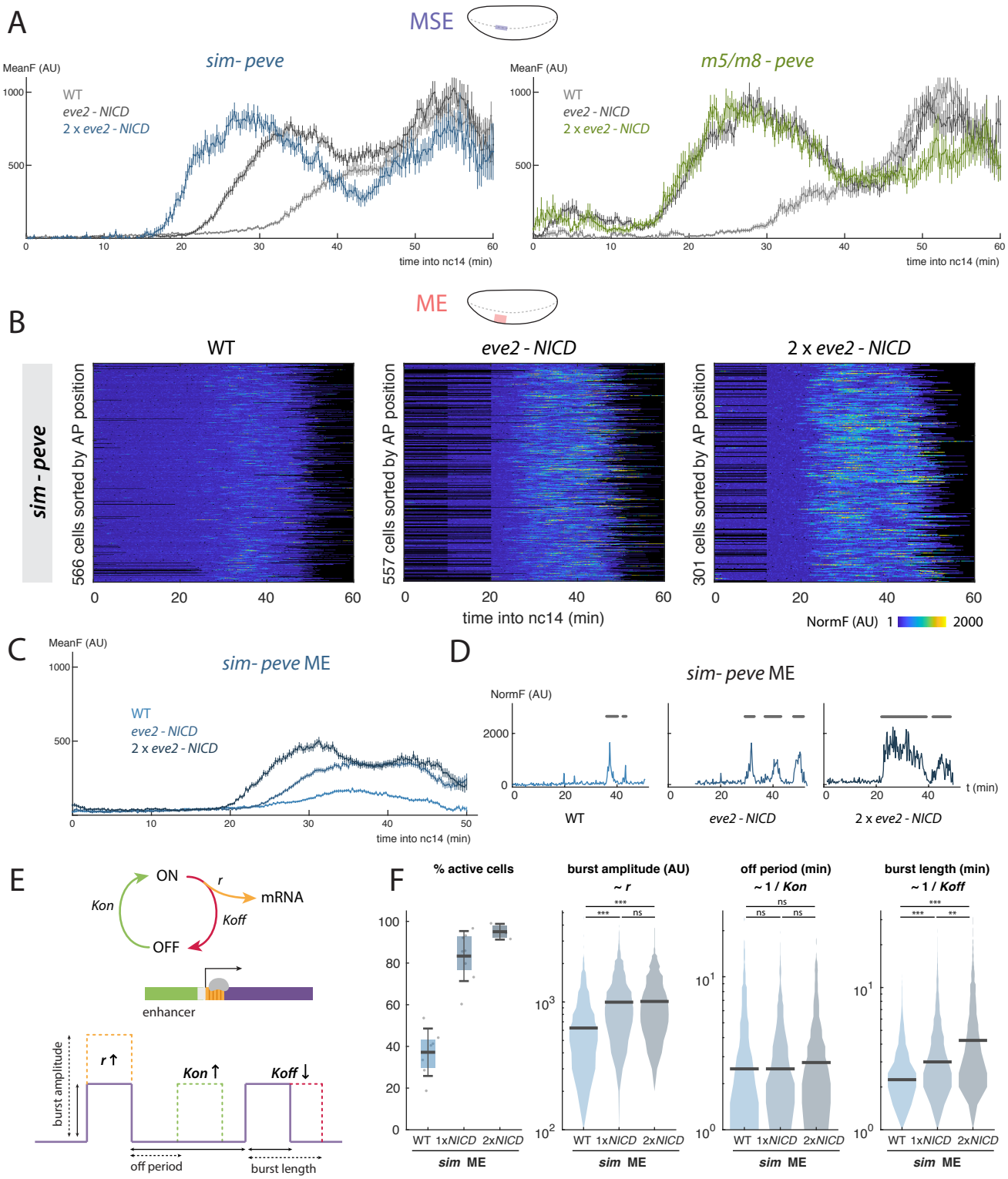

Figure 4. Notch produces a dose-sensitive response by regulating transcription burst size. A) An additional NICD insertion, 2x*eve2-NICD*, elicits earlier and higher transcription from *sim* (blue, left) in MSE cells but does not alter the mean profile from *m5/m8* (green, right) in comparison to 1x*eve2-NICD* (dark grey). Mean levels from wild type (light grey) and 1x*eve2-NICD* (dark grey) embryos are reproduced from Fig. 3**E**. **B**) Heatmaps depicting *sim* activity in ME nuclei in the three conditions as indicated. Note the different scale range compared to Fig. 3**D**. **C**) Ectopic NICD produces a dose-sensitive increase in mean levels of transcription from *sim* in the mesoderm. **D**) Examples of transcription traces from single ME cells in WT, 1x*eve2-NICD* and 2x*eve2-NICD* embryos. Burst periods are marked with a grey line. **E**) Schematic of the model used to describe transcription. An enhancer cycles between ON and OFF states and produces mRNA when

Figure 4 (continued). ON. Changes in the properties of bursting amplidude, off period and bursting length can be correlated with changes in the kinetic constants r, Kon and $Koff$. **F**) Quantification of the bursting properties of transcription from *sim* in mesodermal cells in wild type, 1x*eve2-NICD* and 2x*eve2-NICD* embryos. The proportion of active cells, the burst amplitude and length are all increased but the off period is unchanged. Boxplots indicate median, with 25-75 quartiles; error bars are SD. Violin plots, distributions of the analyzed bursts, bar indicates the median. In **A** and **C** mean fluorescence values and SEM are plotted. n cells for **B**-**F** are indicated in **B**. Differential distributions tested with two-sample Kolmogorov-Smirnov test: pvalues <0.01(*), $<10^{-5}$(**), $<10^{-10}$(***). n = 3 (*m5/m8* 2x*eve2-NICD*), 3 (*sim* 2x*eve2-NICD*) embryos.

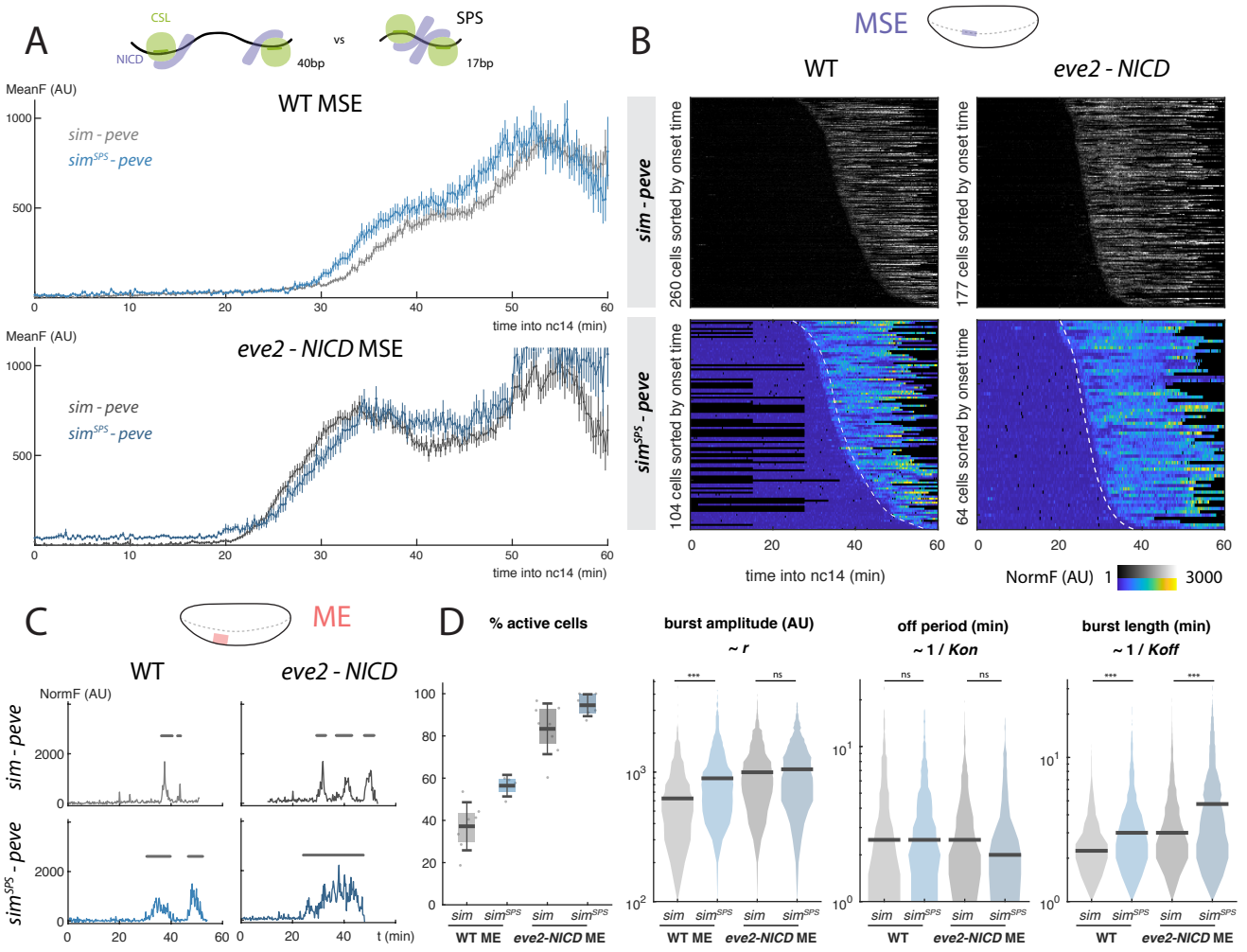

Figure 5. Optimized Su(H) motif organization enhances bursting size. A) Replacing two Su(H) motifs in *sim* with an optimal paired SPS motif sim^{SPS} increases the mean levels of transcription in wild type embryos (top, blue) but does not shift the onset in wild type or *eve2-NICD* embryos (bottom, blue). Mean levels for unmodified *sim* (grey) are from Fig. 3**E**. Mean and SEM for all MSE cells shown. **B**) Heatmaps of transcription in all active MSE cells in the conditions indicated. sim^{SPS} has similar onset to *sim* in wild-type and 1x*eve2-NICD* embryos. **C**) Examples of fluorescent traces from *sim* (grey) and sim^{SPS} (blue) in ME nuclei. Burst periods are indicated with grey lines. **D**) sim^{SPS} induces transcription in a higher proportion of cells and increases the burst size compared to *sim*. Boxplots indicate median, 25-75 quartiles and errorbars are SD. Violin plots, distribution for all bursts measured in the ME, bar indicates the median. Differential distributions tested with two-sample Kolmogorov-Smirnov test: pvalues <0.01(*), $<10^{-5}$(**), $<10^{-10}$(***). n = 4 (sim^{SPS} WT) and 6 (sim^{SPS} *eve2-NICD*) embryos. Grey lines, heatmaps and violin plots are re-plotted from Fig. 3**DE** and 4**DF** for comparison.

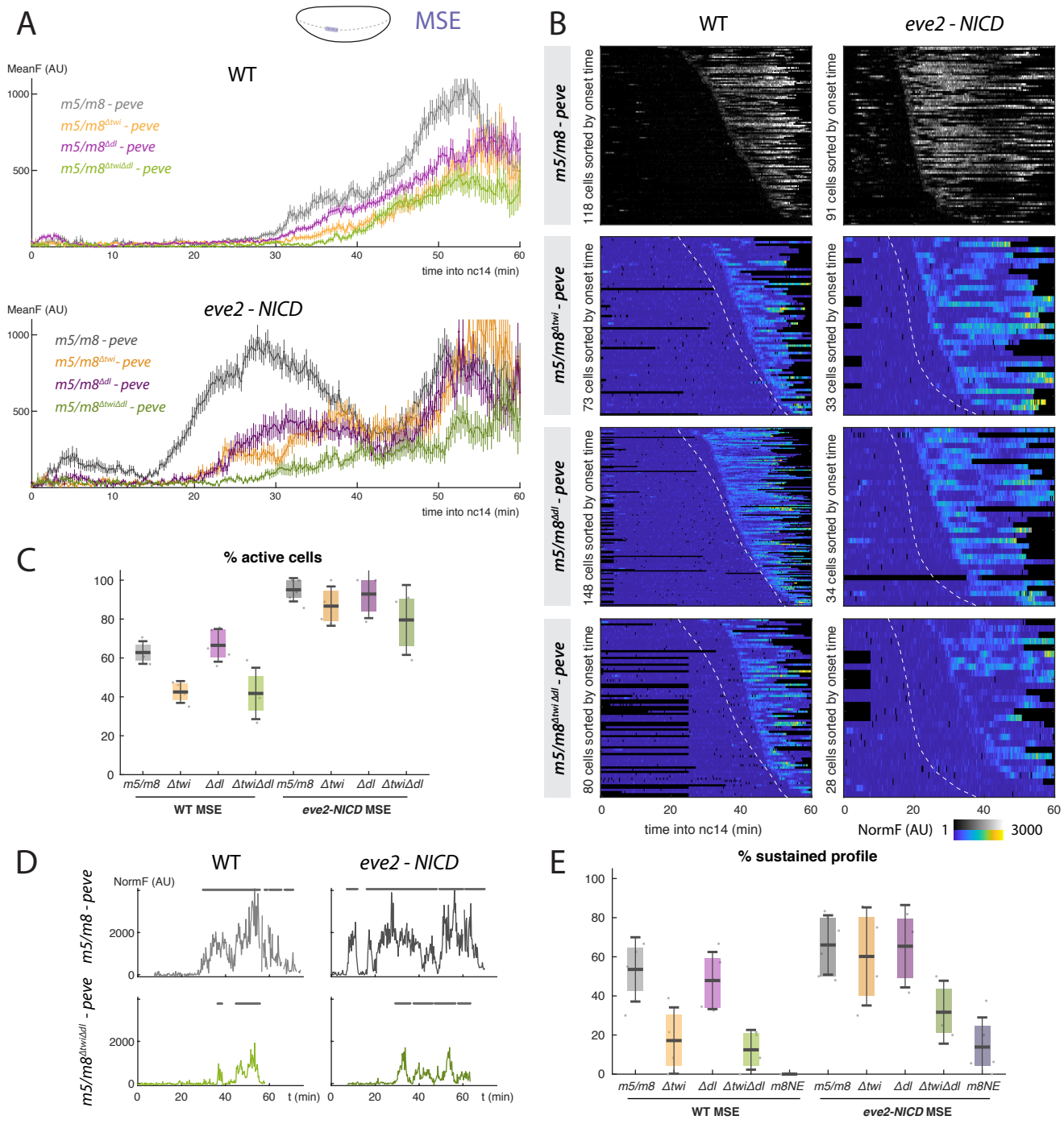

Figure 6. Twist and Dorsal prime the response of *m5/m8* to NICD. A) Mutations in Twist and/or Dorsal binding motifs in *m5/m8* produce delays in the onsets of transcription and lower mean levels of activity in wild type (top) and *eve2-NICD* (bottom) embryos. **B**) Heatmaps of the activity of all MSE cells in the detailed mutated enhancers and conditions. The onset of transcription is delayed when Twist and/or Dorsal motifs are mutated. **C**) Mutations in Twist but not Dorsal motifs reduce the proportion of active cells in wild type embryos. **D**) Examples of transcription traces from MSE cells from the native *m5/m8* enhancer and the enhancer with mutated Twist and Dorsal motifs in wild type and *eve2-NICD* embryos. The profiles from $m5/m8^{\Delta twi\Delta dl}$ MSE cells present 'bursty' rather than sustained transcription. ON periods are marked with a grey line. **E**) Quantification of the proportion of MSE cells per embryo displaying a sustained profile of transcription, defined by the presence of at least one burst longer than 10 min. Median, quartiles and SD are shown. Grey lines and heatmaps are re-plotted from Fig. 3**DE**. n = 4 ($m5/m8^{\Delta twi}$ WT), 5 ($m5/m8^{\Delta dl}$ WT), 4 ($m5/m8^{\Delta twi\Delta dl}$ WT), 4 ($m5/m8^{\Delta twi}$ *eve2-NICD*), 3 ($m5/m8^{\Delta dl}$ *eve2-NICD*), 3 ($m5/m8^{\Delta twi\Delta dl}$ *eve2-NICD*), 3 (*m8NE* WT), 5 (*m8NE eve2-NICD*).

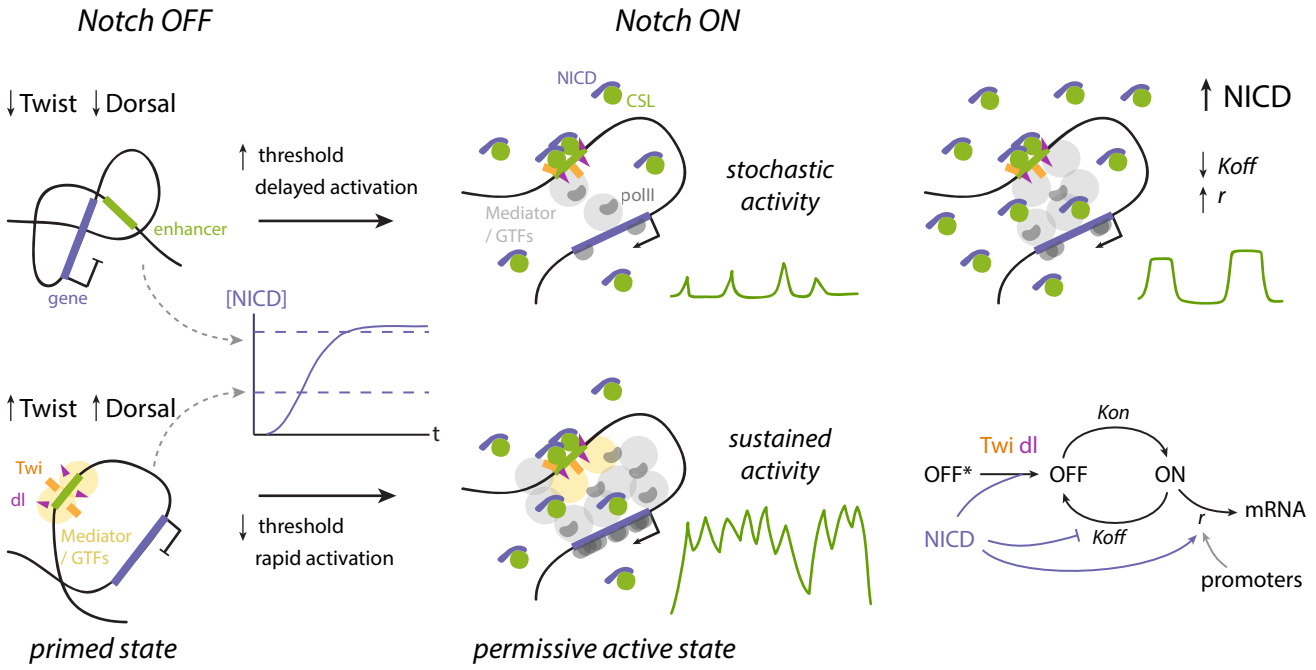

Figure 7. Model of Notch transcriptional regulation through enhancer priming and burst size modulation. Priming by the localized factors Twist and Dorsal produces rapid activation in response to NICD and a state transition into a permissive active state in which sustained transcription can be produced without cycling between on and off states. In the absence of these factors stochastic activity is produced in response to NICD. Increasing levels of NICD regulate the bursting size (higher r and lower K_{off}) and different promoters control the initiation rate r but do not affect the enhancer activation dynamics.

Supporting Information

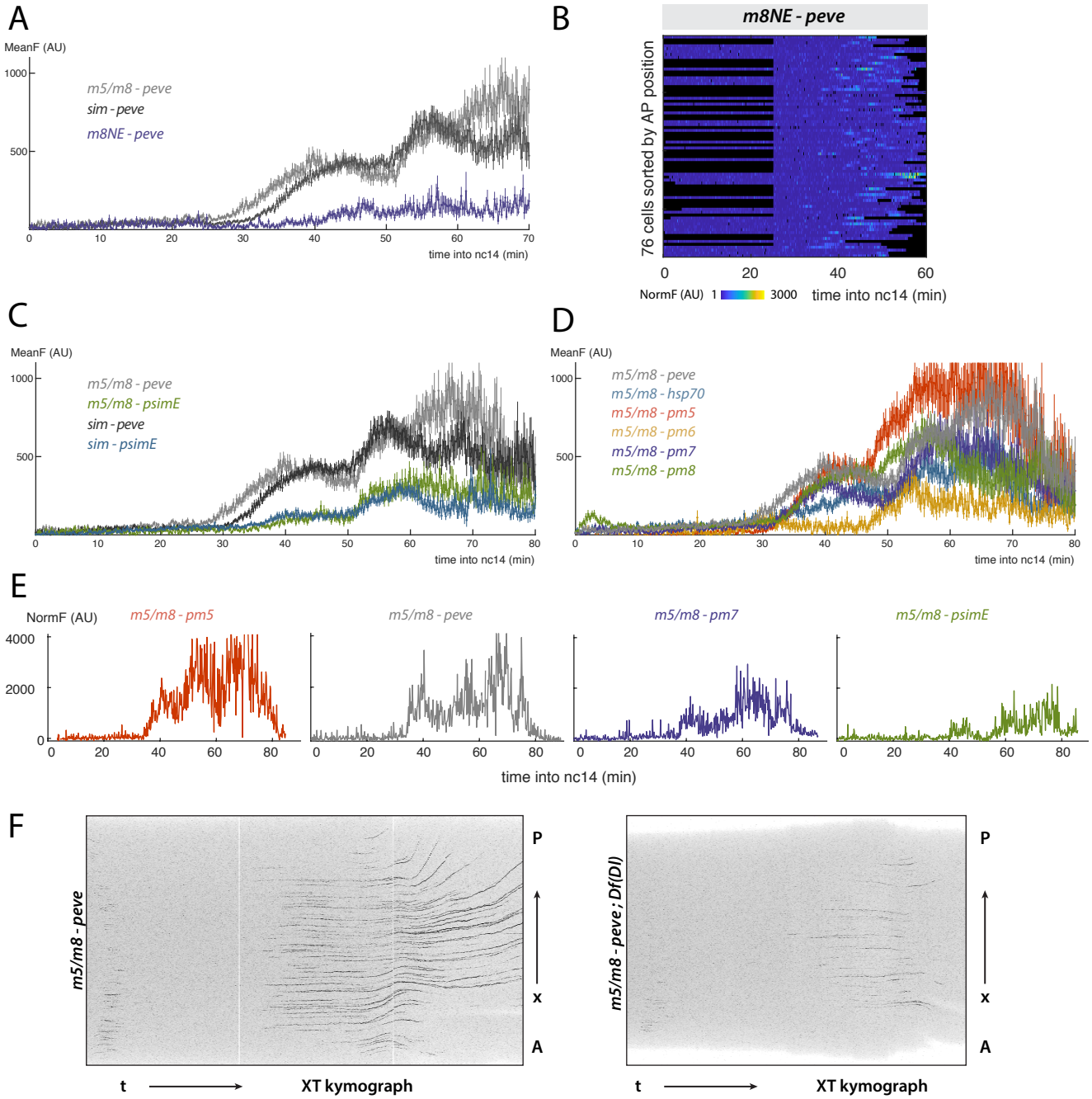

Figure S1. The temporal profile of transcription is characteristic of MSE enhancers. A) A Notch responsive neuroectodermal enhancer (*m8NE*, purple) presents a different temporal pattern than *m5/m8* and *sim*. **B**) *m8NE* produces asynchronized and stochastic transcription in the MSE. **C**) The early promoter of *sim* (*psimE*) produces similar, lower mean levels of transcription from *m5/m8* and *sim* compared to the *eve* promoter. **D**) Different promoters from *E(spl)* complex genes also affect the mean levels of activity but not the global pattern of transcription. **E**) Examples of fluorescent traces from different promoters. All produce continuous traces of different levels. **F**) Projections of the raw MCP-GFP channel over the Y and Z axes creating an XT kymograph. Only a few cells initiate transcription in embryos lacking zygotic Dl protein (right) compared to wild type embryos (left) and it is extinguished earlier. Mean and SEM are shown in **A**, **C** and **D**. Grey lines are re-plotted from Figs. 1**F** 2**A** for comparison. n = 2 (*m8NE-peve*), 2 (*m5/m8-psimE*), 4 (*sim-psimE*), 3 (*m5/m8-hsp70*), 3 (*m5/m8-pm5*), 3 (*m5/m8-pm6*), 3 (*m5/m8-pm7*), 4 (*m5/m8-pm8*).

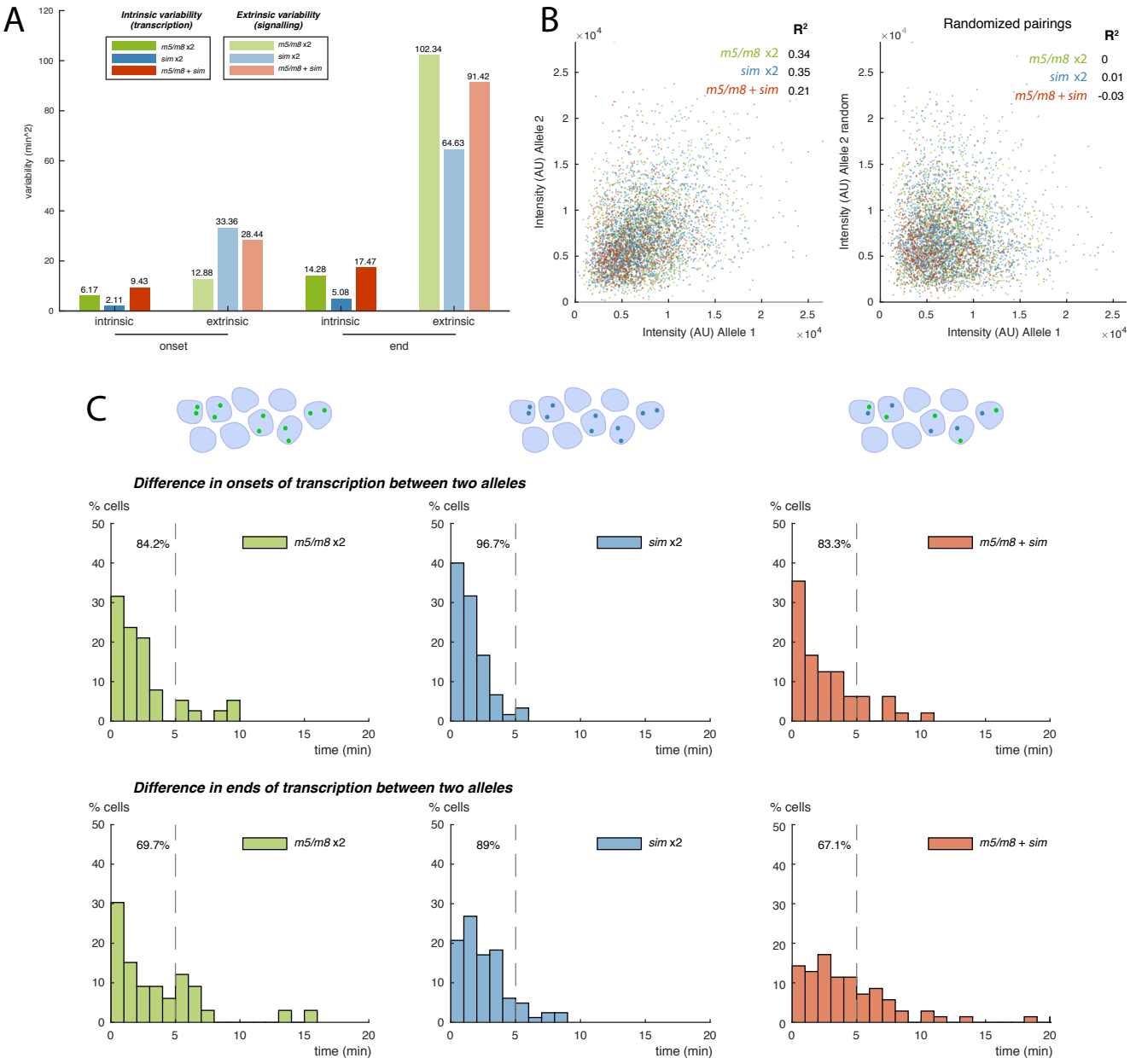

Figure S2. Quantification of the variability intrinsic and extrinsic to transcription. **A**) Intrinsic (total variability minus covariance) and extrinsic (covariance) variability quantified in the onsets and ends of transcription using two MS2 reporters per cell. The amount of intrinsic variability is much smaller than the extrinsic and the intrinsic variability is higher in the ends than onsets of transcription for each combination. **B**) The fluorescence intensities in two alleles at any timepoint present a small but significant correlation (left), compared to a correlation of 0 when the allele pairs are randomly assigned (right). Each color indicates the combination of 2 reporters compared. **C**) Histograms of the time difference between the appearance or dissapearance of transcription foci between the two reporters. The synchrony in the onset times is less than 5 min in more than 80% of the cells and more than 60% in the ends of transcription.

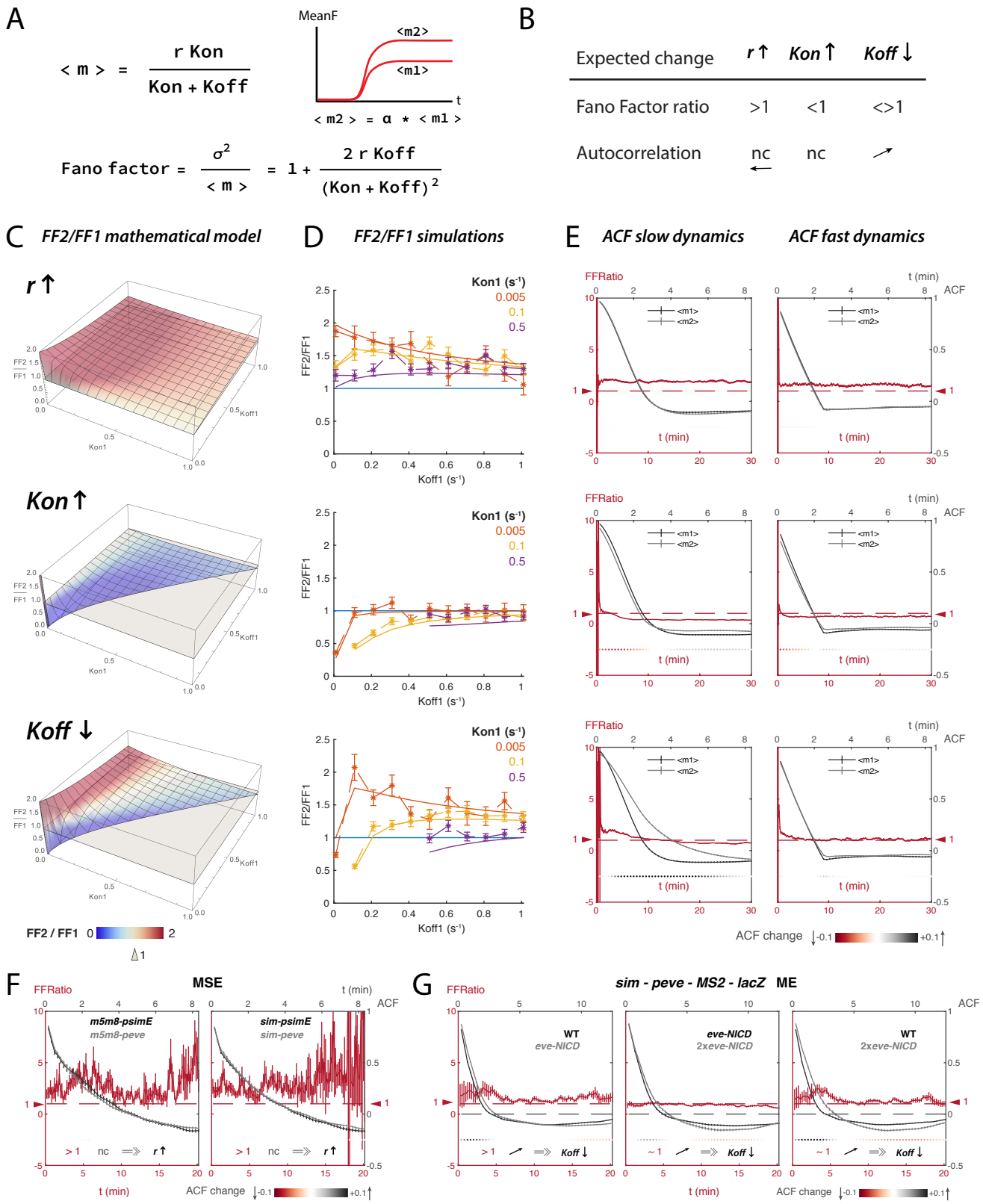

Figure S3. Modelling a two-state promoter to infer changes in the kinetic parameters of transcription. A) Expressions for the mean and Fano Factor of the described 2-state model of transcription. Simulations and experiments compare the traces from two populations that have distinct means $\langle m1 \rangle$ and $\langle m2 \rangle$. α is the fold change in mean levels. **B**) Summary of the effect that affecting r, K_{on} or K_{off} has in the Fano Factor ratio (FF2/FF1) and autocorrelation function (ACF). **C**) 3D plots representing the expected Fano Factor ratio from the mathematical model as a function of K_{on1} and

Figure S3 (continued). K_{off1}. $\alpha = 2$ and $r_1 = 0.3s^{-1}$ in the three plots. When an increase of α in the mean is caused by an increase in r all FF ratio values for any K_{on} and K_{off} values are greater than 1 (top plot). When it is due to an increase in K_{on} all FF ratios are smaller than 1 (middle plot). When K_{off} decreases to produce an increase of α in the mean, the obtained FF ratio values can be greater or smaller than 1 depending on the starting K_{on1} and K_{off1} parameters (bottom plot). The surface plot is colored based on the FF ratio (FF2/FF1) values (blue values close to 0, red close to 2 and white around 1). **D**) Comparisons of the Fano Factor ratios obtained from simulations of MS2 traces with different parameters (dashed lines) and the predicted from the mathematical model (solid line). asterisks and error bars are mean and SD of the Fano Factor ratio over 50 bootstraps of 1000 simulated MS2 traces, using the described K_{on1} and K_{off1} values and $\alpha = 2$, $r_1 = 0.3s^{-1}$, $genelength = 5Kb$, $elongationrate = 2Kb/min$. The expected trends in Fano Factor ratios are correctly recovered in the simulations of transcription. **E**) Changes in the autocorrelation function (ACF) in simulated traces. Mean and SD of the ACF (lag=50) of 1000 simulated MS2 traces in 50 bootstraps, using the described $K_{on1} = 0.005$ and $K_{off1} = 0.01$ (slow dynamics, left column) or $K_{on1} = 0.1$ and $K_{off1} = 0.21$ (fast dynamics, right column) and $\alpha = 2$, $r_1 = 0.3s^{-1}$, $genelength = 5Kb$, $elongationrate = 2Kb/min$. Changes in the ACF are quantified by the difference in the two curves when the errorbars do not overlap, indicated with colored points below each comparison (see scale). No changes are observed when the dynamics are fast. When the dynamics are slow, increases in r do not produce any change in the ACF but changes in K_{on} or K_{off} shift the ACF to the left or right respectively. A greater difference is observed when K_{off} decreases. **F**) Applying the same approach to traces from reporters containing different promoters reveals changes in the mean are due to changes in r (FFRatio greater than 1 and no changes in the ACF). **G**) Comparison of the FF ratio and ACF in ME from *sim* in WT, *eve2-NICD* and 2x*eve2-NICD* reveals changes in the mean are due to a decrease in K_{off} (ACF shifts to the right). **F** and **G** show mean and SD over time of the mean Fano Factor ratio and mean ACF over 50 bootstraps of all traces.

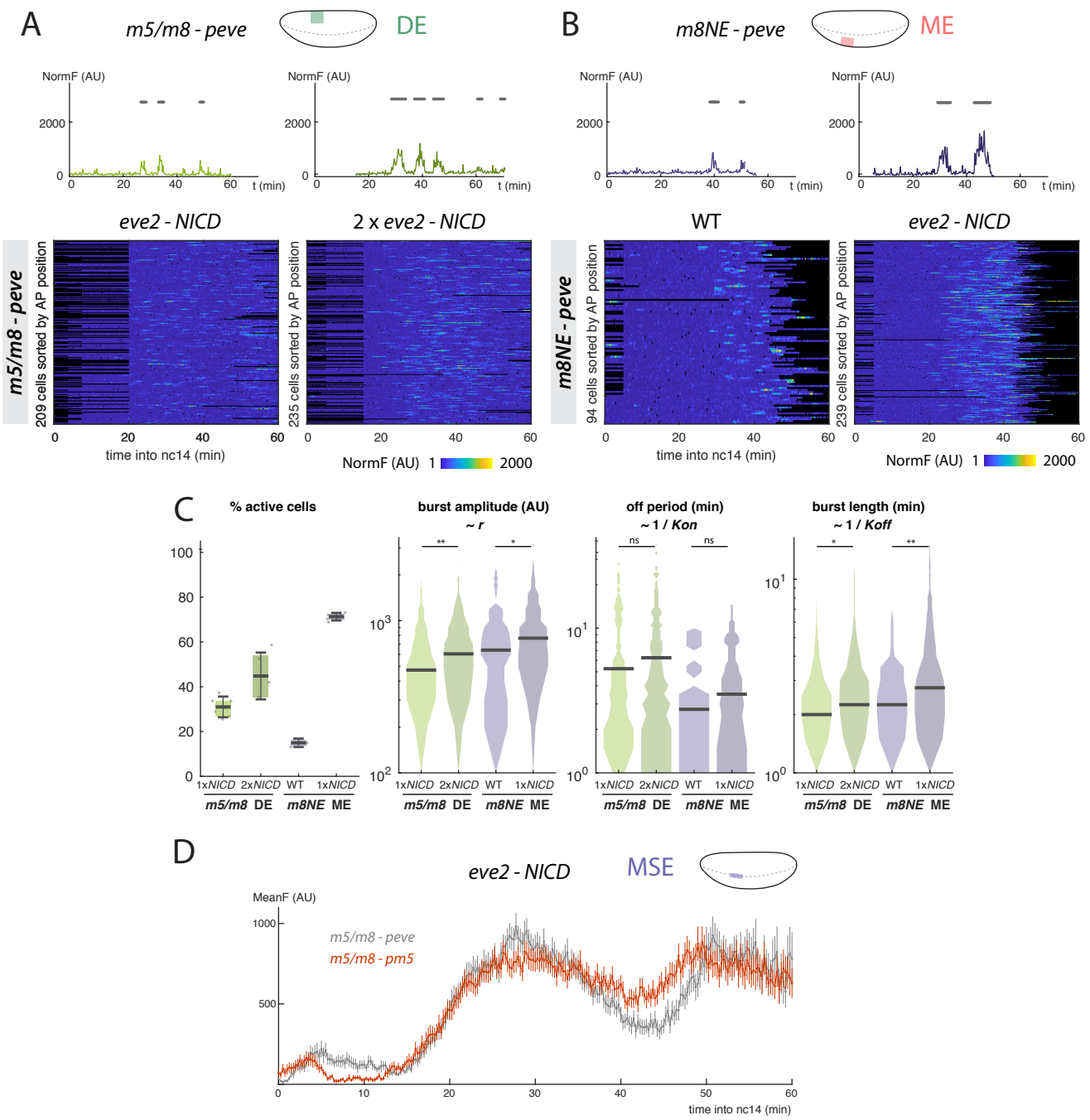

Figure S4. Effects of NICD on the transcriptional bursting properties. **A**) Example traces and heatmaps of cells showing bursts of transcriptional activity from *m5/m8* in the dorsal ectoderm region in conditions of ectopic Notch activity. **B**) Example traces and heatmaps of cells showing bursts of transcriptional activity from *m8NE* in the mesoderm in wild type and *eve2-NICD* embryos. Burst periods are marked with a grey line. **C**) Quantification of the effects of NICD levels on the bursting properties. In both enhancers higher NICD produces a greater proportion of active cells and bigger bursts (increased amplitude and length). **D**) Higher NICD levels saturate the response from the effect on the enhancer. A promoter that produces higher mean levels in wild type embryos does not increase the levels with *eve2-NICD*. Differential distributions in **C** tested with two-sample Kolmogorov-Smirnov test: pvalues <0.01(*), $<10^{-5}$(**), $<10^{-10}$(***). n = 6 (*m5/m8 eve2-NICD* lateral view), 5 (*m5/m8* 2x*eve2-NICD* lateral view), 3 (*m8NE* WT), 5 (*m8NE eve2-NICD*) and 5 (*m5/m8-pm5 eve2-NICD*) embryos. Grey lines in **D** are re-plotted from Fig. 3**E**.

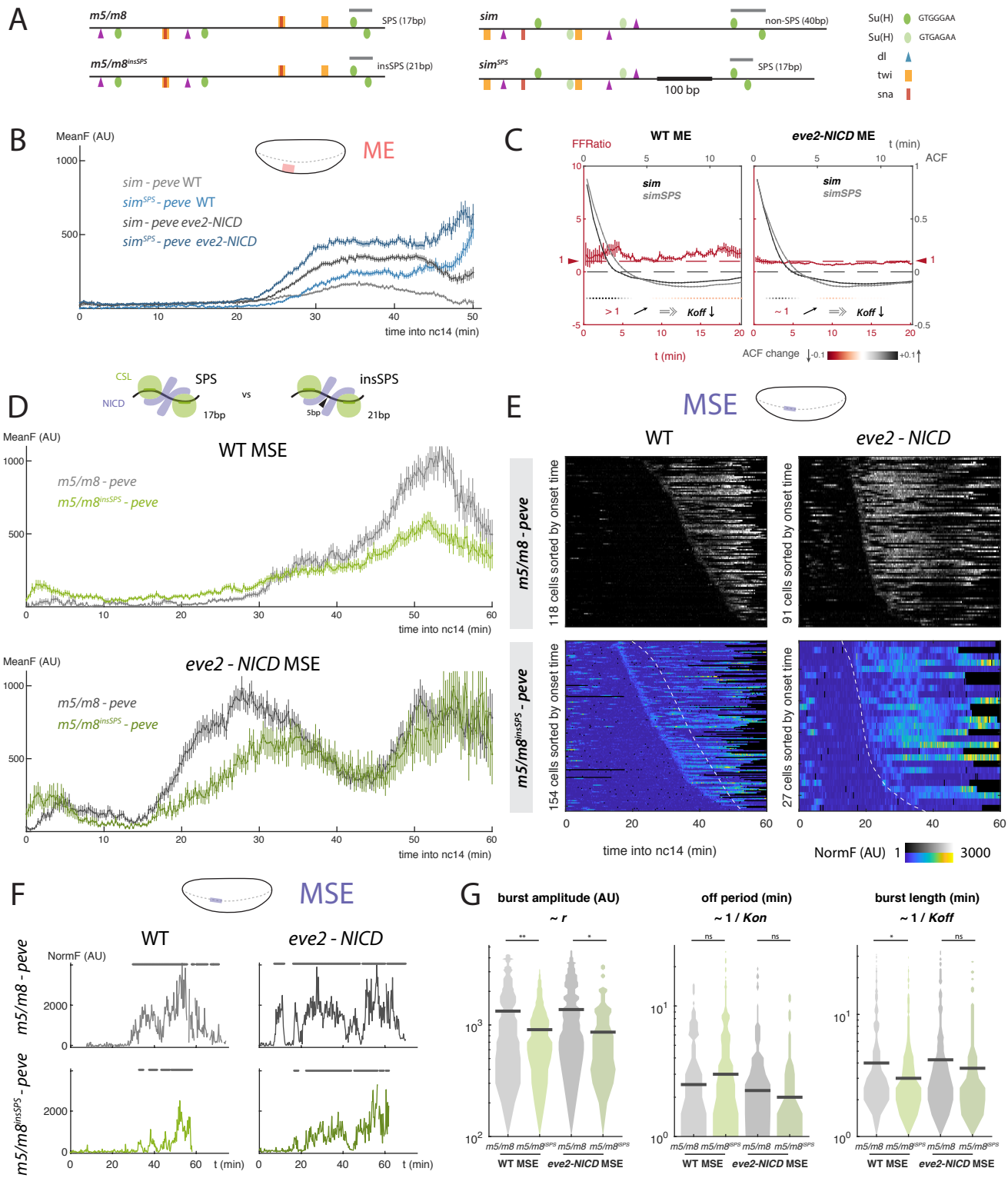

Figure S5. Disruption of a SPS site produces lower transcription levels but does not delay the onset of transcription. **A**) Schematic representation of Su(H), Dorsal, Twist and Snail binding motifs in *m5/m8* and *sim* and introduced alterations in the SPS sites. **B**) sim^{SPS} produces higher mean levels in the mesoderm compared to *sim*, in both wild type and *eve2-NICD* embryos. **C**) The Fano Factor ratio and autocorrelation function of *sim* and sim^{SPS} traces in the mesoderm in wild type and *eve2-NICD* embryos are compatible with changes in $Koff$ to produce increases in mean levels from *sim* to sim^{SPS}, in agreement with 5**D**. **D**) $m5/m8^{insSPS}$ produces lower mean levels of transcription compared to *m5/m8* but does not delay the onset of the response. **E**) $m5/m8^{ins}$ does not shift the onset of the response in *eve2-NICD* embryos compared to *m5/m8* but presents some de-repression in wild type embryos. **F**) Examples of fluorescent traces in the

Figure S5 (continued). mesectoderm region in the described conditions. Burst periods are marked with a grey line. **G**) Quantification of the busting properties in the mesectoderm. $m5/m8^{insSPS}$ produces smaller bursts (lower amplitude and shorter length) than *m5/m8*. Differential distributions in **G** tested with two-sample Kolmogorov-Smirnov test: pvalues <0.01(*), $<10^{-5}$(**), $<10^{-10}$(***). n = 5 ($m5/m8^{insSPS}$ WT), 3 ($m5/m8^{insSPS}$ *eve2-NICD*). Grey lines and heatmaps in **DE** are re-plotted from Fig. 3**ED**. **C** shows mean and SD over time of the mean Fano Factor ratio and mean ACF over 50 bootstraps of all traces.

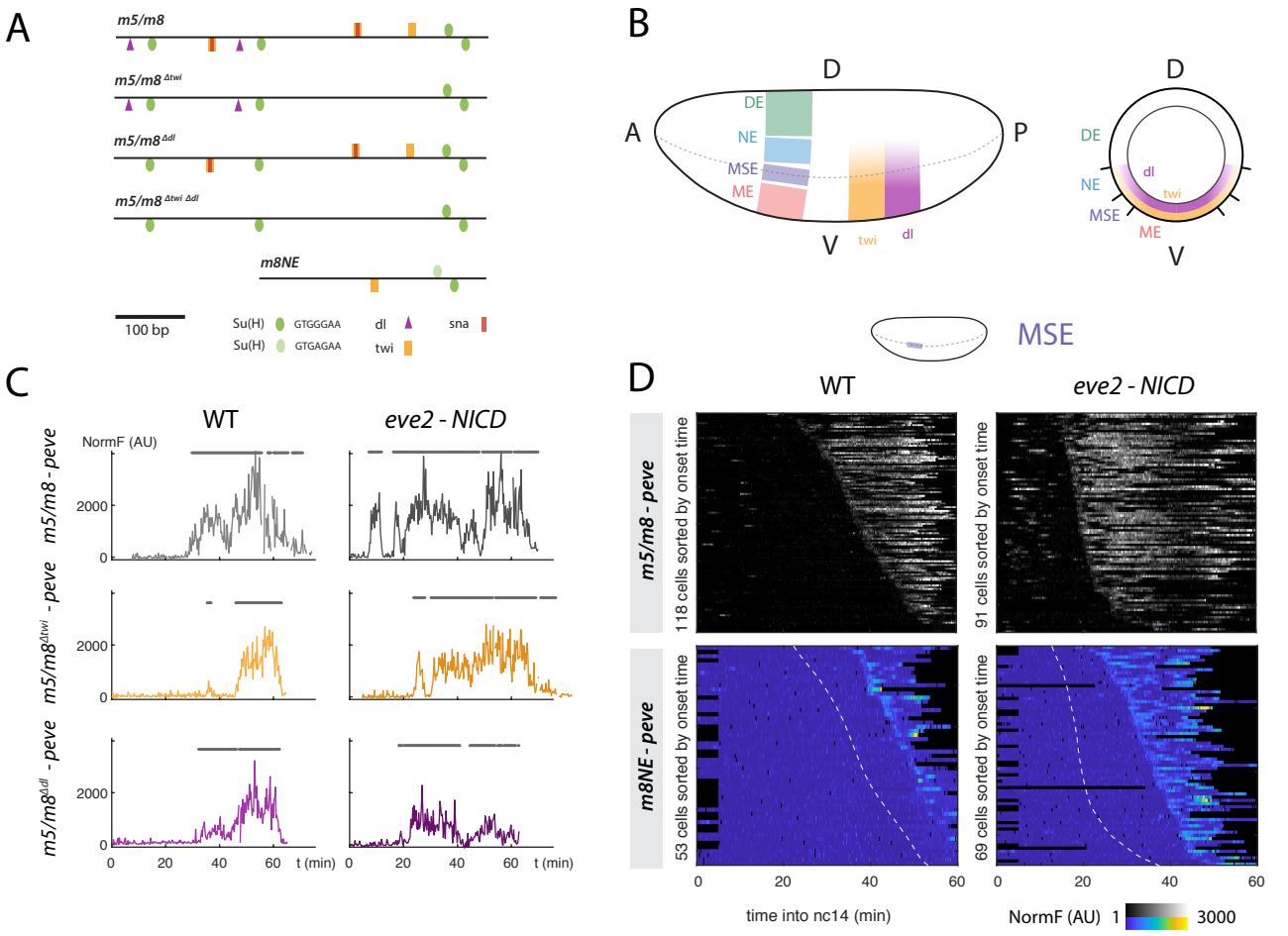

Figure S6. Effects of mutations in Twist and Dorsal in the onset of transcription. A) Schematic representation of the introduced mutations in *m5/m8* and comparison with a neuroectodermal enhancer, *m8NE*. **B**) Diagram of Twist and Dorsal gradients in the blastoderm embryo. Both extend in a ventral to dorsal gradient in the ME, MSE and NE. **C**) Examples of transcription traces from mesectodermal cells expressing *m5/m8* with mutated Twist or Dorsal motifs. The onset of transcription is delayed but transcrtiption still occurs in a sustained manner. **D**) Heatmaps of MSE cells expressing *m8NE*. The onset of transcription is delayed compared to *m5/m8*.

Supplementary movies

Movie 1. Expression of *m5/m8-peve*.

Movie 2. Expression of *sim-peve*.

Movie 3. Ectopic expression with *eve2-NICD*.

Acknowledgments

566

References

[1] A. M. Bailey and J. W. Posakony. Supressor of Hairless directly activates transcription of Enhacer of split Complex genes in response to Notch receptor activity. *Gen. & Dev.*, (9):2609–2622, 1995.

[2] C. R. Bartman, S. C. Hsu, C. C. Hsiung, A. Raj, G. A. Blobel, C. R. Bartman, S. C. Hsu, C. C. Hsiung, A. Raj, and G. A. Blobel. Enhancer Regulation of Transcriptional Bursting Parameters Revealed by Forced Chromatin Looping. *Molecular Cell*, pages 1–11, 2016.

[3] C. R. Bartman, S. C. Hsu, C. C. S. Hsiung, A. Raj, and G. A. Blobel. Enhancer Regulation of Transcriptional Bursting Parameters Revealed by Forced Chromatin Looping. *Molecular Cell*, 62(2):237–247, 2016.

[4] A. Berrocal, N. Lammers, H. G. Garcia, and M. B. Eisen. Kinetic sculpting of the seven stripes of the Drosophila even-skipped gene. 2018.

[5] J. Bischof, M. Björklund, E. Furger, C. Schertel, J. Taipale, K. Basler, K. Basler, G. Struhl, J. R. Bateman, A. M. Lee, C. T. Wu, H. J. Bellen, R. W. Levis, Y. He, J. W. Carlson, M. Evans-Holm, E. Bae, J. Kim, A. Metaxakis, C. Savakis, K. L. Schulze, J. Bischof, R. K. Maeda, M. Hediger, F. Karch, K. Basler, M. Björklund, M. Taipale, M. Varjosalo, J. Saharinen, J. Lahdenperä, J. Taipale, A. H. Brand, N. Perrimon, S. P. Brothers, J. A. Janovick, P. M. Conn, E. Caussinus, O. Kanca, M. Affolter, D. R. Cavener, G. Dietzl, D. Chen, F. Schnorrer, K. C. Su, Y. Barinova, M. Fellner, B. Gasser, K. Kinsey, S. Oppel, S. Scheiblauer, A. C. Groth, M. Fish, R. Nusse, M. P. Calos, I. Herskowitz, C. Horn, B. Jaunich, E. A. Wimmer, C. D. Hu, Y. Chinenov, T. K. Kerppola, F. Jankovics, D. Brunner, J. W. Jarvik, C. A. Telmer, T. J. Jaw, L. R. You, P. S. Knoepfler, L. C. Yao, C. Y. Pai, C. Y. Tang, L. P. Chang, J. Berthelsen, F. Blasi, M. P. Kamps, S. L. Lai, T. Lee, C. Larsen, X. Franch-Marro, V. Hartenstein, C. Alexandre, J. P. Vincent, T. Lee, L. Luo, G. L. Miklos, G. M. Rubin, A. L. Parks, K. R. Cook, M. Belvin, N. A. Dompe, R. Fawcett, K. Huppert, L. R. Tan, C. G. Winter, K. P. Bogart, J. E. Deal, G. Prelich, A. K. Ramani, T. Chuluunbaatar, A. J. Verster, H. Na, V. Vu, N. Pelte, N. Wannissorn, A. Jiao, A. G. Fraser, J. D. Romano, W. K. Schmidt, S. Michaelis, P. Rørth, Y. Saka, A. I. Hagemann, O. Piepenburg, J. C. Smith, C. Schertel, D. Huang, M. Björklund, J. Bischof, D. Yin, R. Li, Y. Wu, R. Zeng, J. Wu, J. Taipale, T. Schlake, J. Bode, C. Taxis, G. Stier, R. Spadaccini, M. Knop, K. J. Venken, Y. He, R. A. Hoskins, H. J. Bellen, K. J. Venken, J. H. Simpson, H. J. Bellen, I. Viktorinová, E. A. Wimmer, N. Wei, G. Serino, X. W. Deng, F. Wittwer, M. Jaquenoud, W. Brogiolo, M. Zarske, P. Wüstemann, R. Fernandez, H. Stocker, M. P. Wymann, E. Hafen, R. Xu, K. Deng, Y. Zhu, Y. Wu, J. Ren, M. Wan, S. Zhao, X. Wu, M. Han, Y. Zhuang, R. Yagi, F. Mayer, K. Basler, C. Yu, K. H. Wan, A. S. Hammonds, M. Stapleton, J. W. Carlson, S. E. Celniker, J. Zhong, and B. Yedvobnick. A versatile platform for creating a comprehensive UAS-ORFeome library in Drosophila. *Development (Cambridge, England)*, 140(11):2434–42, 2013.

[6] J. Bischof, R. K. Maeda, M. Hediger, F. Karch, and K. Basler. An optimized transgenesis system for Drosophila using germ-line-specific phiC31 integrases. *Proceedings of the National Academy of Sciences of the United States of America*, 104(9):3312–7, 2007.

[7] A. Boija, I. A. Klein, B. R. Sabari, A. Dall'Agnese, E. L. Coffey, A. V. Zamudio, C. H. Li, K. Shrinivas, J. C. Manteiga, N. M. Hannett, B. J. Abraham, L. K. Afeyan, Y. E. Guo, J. K. Rimel, C. B. Fant, J. Schuijers, T. I. Lee, D. J. Taatjes, and R. A. Young. Transcription Factors Activate Genes through the Phase-Separation Capacity of Their Activation Domains. *Cell*, pages 1–14, 2018.

[8] H. Boije, S. Rulands, S. Dudczig, B. D. Simons, and W. A. Harris. The Independent Probabilistic Firing of Transcription Factors: A Paradigm for Clonal Variability in the Zebrafish Retina. *Developmental Cell*, 34(5):532–543, 2015.

[9] J. P. Bothma, H. G. Garcia, E. Esposito, G. Schlissel, T. Gregor, and M. Levine. Dynamic regulation of eve stripe 2 expression reveals transcriptional bursts in living Drosophila embryos. *Proceedings of the National Academy of Sciences*, 111(29):10598–10603, 2014.

[10] J. P. Bothma, M. R. Norstad, S. Alamos, and H. G. Garcia. LlamaTags: A Versatile Tool to Image Transcription Factor Dynamics in Live Embryos. *Cell*, pages 1–13, 2018.

[11] S. J. Bray. Notch signalling: a simple pathway becomes complex. *Nature reviews. Molecular cell biology*, 7(9):678–89, sep 2006.

[12] H. H. Chang, M. Hemberg, M. Barahona, D. E. Ingber, and S. Huang. Transcriptome-wide noise controls lineage choice in mammalian progenitor cells. *Nature*, 453(7194):544–547, 2008.

[13] W.-k. Cho, N. Jayanth, B. P. English, T. Inoue, J. O. Andrews, W. Conway, J. B. Grimm, J.-h. Spille, L. D. Lavis, T. Lionnet, and I. I. Cisse. RNA Polymerase II cluster dynamics predict mRNA output in living cells. *eLife*, 5:1–31, may 2016.

[14] W. K. Cho, J. H. Spille, M. Hecht, C. Lee, C. Li, V. Grube, and I. I. Cisse. Mediator and RNA polymerase II clusters associate in transcription-dependent condensates. *Science*, 361(6400):412–415, 2018.

[15] J. R. Chubb, T. Trcek, S. M. Shenoy, and R. H. Singer. Transcriptional Pulsing of a Developmental Gene. *Current Biology*, 16(10):1018–1025, 2006.

[16] J. Cowden and M. Levine. The Snail repressor positions Notch signaling in the Drosophila embryo. *Development (Cambridge, England)*, 129(7):1785–1793, 2002.

[17] R. D. Dar, B. S. Razooky, A. Singh, T. V. Trimeloni, J. M. McCollum, C. D. Cox, M. L. Simpson, and L. S. Weinberger. Transcriptional burst frequency and burst size are equally modulated across the human genome. *Proceedings of the National Academy of Sciences*, 109(43):17454–17459, 2012.

[18] S. De Renzis, J. Yu, R. Zinzen, and E. Wieschaus. Dorsal-Ventral Pattern of Delta Trafficking Is Established by a Snail-Tom-Neuralized Pathway. 2006.

[19] J. Desponds, H. Tran, T. Ferraro, T. Lucas, C. Perez Romero, A. Guillou, C. Fradin, M. Coppey, N. Dostatni, and A. M. Walczak. Precision of Readout at the hunchback Gene: Analyzing Short Transcription Time Traces in Living Fly Embryos. *PLOS Computational Biology*, 12(12):e1005256, dec 2016.

[20] C. Fritzsch, S. Baumgärtner, M. Kuban, D. Steinshorn, G. Reid, and S. Legewie. Estrogen-dependent control and cell-to-cell variability of transcriptional bursting. *Molecular Systems Biology*, 14(2):e7678, 2018.

[21] T. Fukaya, B. Lim, and M. Levine. Enhancer Control of Transcriptional Bursting. *Cell*, 166:1–11, 2016.

[22] H. Garcia, M. Tikhonov, A. Lin, and T. Gregor. Quantitative Imaging of Transcription in Living Drosophila Embryos Links Polymerase Activity to Patterning. *Current Biology*, 23(21):2140–2145, 2013.

[23] D. G. Gibson. Enzymatic Assembly of Overlapping DNA Fragments. 498:349–361, 2011.

[24] D. T. Gillespie. A general method for numerically simulating the stochastic time evolution of coupled chemical reactions. *Journal of Computational Physics*, 22(4):403–434, dec 1976.

[25] I. Golding, J. Paulsson, S. M. Zawilski, and E. C. Cox. Real-time kinetics of gene activity in individual bacteria. *Cell*, 123(6):1025–1036, 2005.

[26] M. J. Gomez-Lamarca, J. Falo-Sanjuan, R. Stojnic, S. Abdul Rehman, L. Muresan, M. L. Jones, Z. Pillidge, G. Cerda-Moya, Z. Yuan, S. Baloul, P. Valenti, K. Bystricky, F. Payre, K. O'Holleran, R. Kovall, and S. J. Bray. Activation of the Notch Signaling Pathway In Vivo Elicits Changes in CSL Nuclear Dynamics. *Developmental Cell*, 44(5):611–623.e7, mar 2018.

[27] C. V. Harper, B. Finkenstädt, D. J. Woodcock, S. Friedrichsen, S. Semprini, L. Ashall, D. G. Spiller, J. J. Mullins, D. A. Rand, J. R. E. Davis, and M. R. H. White. Dynamic analysis of stochastic transcription cycles. *PLoS Biology*, 9(4), 2011.

[28] C. C. Kopczynski, A. K. Alton, K. Fechtel, P. J. Kooh, and M. A. Muskavitch. Delta, a Drosophila neurogenic gene, is transcriptionally complex and encodes a protein related to blood coagulation factors and epidermal growth factor of vertebrates. *Genes & development*, 2(12 B):1723–1735, 1988.

[29] D. Kosman and S. Small. Concentration-dependent patterning by an ectopic expression domain of the Drosophila gap gene knirps. *Development (Cambridge, England)*, 124(7):1343–1354, 1997.

[30] B. Kramatschek and J. a. Campos-Ortega. Neuroectodermal transcription of the Drosophila neurogenic genes E(spl) and HLH-m5 is regulated by proneural genes. *Development (Cambridge, England)*, 120(4):815–826, 1994.

[31] N. C. Lammers, V. Galstyan, A. Reimer, S. A. Medin, C. H. Wiggins, and H. G. Garcia. Binary transcriptional control of pattern formation in development. *bioRxiv*, page 335919, 2018.

[32] D. R. Larson, C. Fritzsch, L. Sun, X. Meng, D. S. Lawrence, and R. H. Singer. Direct observation of frequency modulated transcription in single cells using light activation. *eLife*, 2013(2):1–20, 2013.

[33] D. R. Larson, R. H. Singer, and D. Zenklusen. A single molecule view of gene expression. *Trends in Cell Biology*, 19(11):630–637, 2009.

[34] S. C. Little, M. Tikhonov, and T. Gregor. Precise developmental gene expression arises from globally stochastic transcriptional activity. *Cell*, 154(4):789–800, 2013.

[35] H. Lu, D. Yu, A. S. Hansen, S. Ganguly, R. Liu, A. Heckert, X. Darzacq, and Q. Zhou. Phase-separation mechanism for C-terminal hyperphosphorylation of RNA polymerase II. *Nature*, 1, 2018.

[36] M. Mir, A. Reimer, J. E. Haines, X.-y. Li, M. Stadler, H. Garcia, M. B. Eisen, and X. Darzacq. Dense Bicoid hubs accentuate binding along the morphogen gradient. pages 1784–1794, 2017.

[37] Y. Mishchenko. A fast algorithm for computation of discrete Euclidean distance transform in three or more dimensions on vector processing architectures. *Signal, Image and Video Processing*, 9(1):19–27, jan 2015.

[38] V. Morel, R. Le Borgne, and F. Schweisguth. Snail is required for Delta endocytosis and Notch-dependent activation of single-minded expression. *Development genes and evolution*, 213(2):65–72, 2003.

[39] V. Morel and F. Schweisguth. Repression by Suppressor of Hairless and activation by Notch are required to define a single row of single-minded expressing cells in the Drosophila embryo. *Genes and Development*, 14(3):377–388, 2000.

[40] Y. Nam, P. Sliz, W. S. Pear, J. C. Aster, and S. C. Blacklow. Cooperative assembly of higher-order Notch complexes functions as a switch to induce transcription. *Proceedings of the National Academy of Sciences of the United States of America*, 104(7):2103–8, 2007.

[41] N. Nandagopal, L. A. Santat, L. LeBon, D. Sprinzak, M. E. Bronner, and M. B. Elowitz. Dynamic Ligand Discrimination in the Notch Signaling Pathway. *Cell*, 172(4):869–880.e19, feb 2018.

[42] K. K. H. Ng, M. A. Yui, A. Mehta, S. Siu, B. Irwin, S. Pease, S. Hirose, M. B. Elowitz, E. V. Rothenberg, and H. Y. Kueh. A stochastic epigenetic switch controls the dynamics of T-cell lineage commitment. pages 1–38, 2018.

[43] J. Peccoud and B. Ycart. Markovian modelling of gene products synthesis, 1995.

[44] A. Raj and A. van Oudenaarden. Nature, Nurture, or Chance: Stochastic Gene Expression and Its Consequences. *Cell*, 135(2):216–226, 2008.

[45] B. R. Sabari, A. Dall'Agnese, A. Boija, I. A. Klein, E. L. Coffey, K. Shrinivas, B. J. Abraham, N. M. Hannett, A. V. Zamudio, J. C. Manteiga, C. H. Li, Y. E. Guo, D. S. Day, J. Schuijers, E. Vasile, S. Malik, D. Hnisz, T. I. Lee, I. I. Cisse, R. G. Roeder, P. A. Sharp, A. K. Chakraborty, and R. A. Young. Coactivator condensation at super-enhancers links phase separation and gene control. *Science*, 361(6400), 2018.

[46] A. Senecal, B. Munsky, F. Proux, N. Ly, F. E. Braye, C. Zimmer, F. Mueller, and X. Darzacq. Transcription factors modulate c-Fos transcriptional bursts. *Cell Reports*, 8(1):75–83, 2014.

[47] K. Tantale, F. Mueller, A. Kozulic-Pirher, A. Lesne, J. M. Victor, M. C. Robert, S. Capozi, R. Chouaib, V. Bäcker, J. Mateos-Langerak, X. Darzacq, C. Zimmer, E. Basyuk, and E. Bertrand. A single-molecule view of transcription reveals convoys of RNA polymerases and multi-scale bursting. *Nature Communications*, 7, 2016.

[48] A. Tsai, A. K. Muthusamy, M. R. P. Alves, L. D. Lavis, R. H. Singer, D. L. Stern, and J. Crocker. Nuclear microenvironments modulate transcription from low-affinity enhancers. pages 1–18, 2017.

[49] H. Vässin and J. A. Campos-Ortega. Genetic Analysis of Delta, a Neurogenic Gene of Drosophila melanogaster. *Genetics*, 116(3):433–45, jul 1987.

[50] M. F. Wernet, E. O. Mazzoni, A. Çelik, D. M. Duncan, I. Duncan, and C. Desplan. Stochastic spineless expression creates the retinal mosaic for colour vision. *Nature*, 440(7081):174–180, 2006.

[51] M. a. Zabidi, C. D. Arnold, K. Schernhuber, M. Pagani, M. Rath, O. Frank, and A. Stark. Enhancer—core-promoter specificity separates developmental and housekeeping gene regulation. *Nature*, 518(7540):556–559, 2014.

[52] R. P. Zinzen, J. Cande, M. Ronshaugen, D. Papatsenko, and M. Levine. Evolution of the Ventral Midline in Insect Embryos. 2006.

[53] R. P. Zinzen, K. Senger, M. Levine, and D. Papatsenko. Computational Models for Neurogenic Gene Expression in the Drosophila Embryo. *Current Biology*, 16(13):1358–1365, 2006.